Chemical Geology 471 (2017) 74–91

Contents lists available at ScienceDirect

Chemical Geology

journal homepage: www.elsevier.com/locate/chemgeo

Stream and slope weathering effects on organic-rich mudstone geochemistry and implications for hydrocarbon source rock assessment: A Bowland Shale case study

Joseph F. Emmings[a,*], Sarah J. Davies[a], Christopher H. Vane[b], Melanie J. Leng[c,d], Vicky Moss-Hayes[b], Michael H. Stephenson[b], Gawen R.T. Jenkin[a]

[a] School of Geography, Geology and the Environment, University of Leicester, University Road, Leicester LE1 7RH, UK
[b] British Geological Survey, Keyworth, Nottingham NG12 5GG, UK
[c] NERC Isotopes Geosciences Facilities, British Geological Survey, Keyworth, Nottingham NG12 5GG, UK
[d] Centre for Environmental Geochemistry, University of Nottingham, Nottingham NG7 2RD, UK

ARTICLE INFO

Editor: G. Jerome

Keywords:
Bowland
Shale
Weathering
Rock-Eval
Organic-rich

ABSTRACT

This study contributes to the exploration and quantification of the weathering of organic-rich mudstones under temperate climatic conditions. Bowland Shales, exposed by a stream and slope, were sampled in order to develop a model for the effects of weathering on the mudstone geochemistry, including major and trace element geochemistry, Rock-Eval pyrolysis and $\delta^{13}C_{org}$. Four weathering grades (I – IV) are defined using a visual classification scheme; visually fresh and unaltered (I), chemically altered (II, III) and 'paper shale' that typifies weathered mudstone on slopes (IV). Bedload abrasion in the stream exposes of visually fresh and geochemically unaltered mudstone. Natural fractures are conduits for oxidising meteoric waters that promote leaching at the millimetre scale and/or precipitation of iron oxide coatings along fracture surfaces. On the slope, bedding-parallel fractures formed (and may continue to form) in response to chemical and/or physical weathering processes. These fractures develop along planes of weakness, typically along laminae comprising detrital grains, and exhibit millimetre- and centimetre-scale leached layers and iron oxide coatings. Fracture surfaces are progressively exposed to physical weathering processes towards the outcrop surface, and results in disintegration of the altered material along fracture surfaces. Grade IV, 'paper shale' mudstone is chemically unaltered but represents a biased record driven by initial heterogeneity in the sedimentary fabric. Chemically weathered outcrop samples exhibit lower concentrations of both 'free' (S1) (up to 0.6 mgHC/g rock) and 'bound' (S2) (up to 3.2 mgHC/g rock) hydrocarbon, reduced total organic carbon content (up to 0.34 wt%), reduced hydrogen index (up to 58 mgHC/gTOC), increased oxygen index (up to 19 mgCO + CO_2/gTOC) and increased T_{max} (up to 11 °C) compared with unaltered samples. If analysis of chemically weathered samples is unavoidable, back-extrapolation of Rock-Eval parameters can assist in the estimation of pre-weathering organic compositions. Combining Cs/Cu with oxygen index is a proxy for identifying the weathering progression from fresh material (I) to 'paper shale' (IV). This study demonstrates that outcrop samples in temperate climates can provide information for assessing hydrocarbon potential of organic-rich mudstones.

1. Introduction

Organic-rich mudstones are prone to physical and chemical alteration at outcrop because they contain components that are out of chemical equilibrium with present day surface oxidising conditions (e.g., Goldich, 1938; White and Buss, 2013). In order to avoid any detrimental effects of modern weathering, geochemical studies of organic-rich mudstones preferentially focus on samples obtained from borehole core samples located sufficiently far from the surficial weathered zone. However, where borehole core material is not available or practical to acquire, analysis of samples is by necessity conducted on those collected from outcrop.

The Mississippian Craven Basin, UK, is an example of an emerging hydrocarbon province that includes many exposures that dissect the basin. These exposures include the organic-rich Bowland Shale that may represent a significant unconventional hydrocarbon resource (Andrews, 2013). However, uncertainties exist, such as variable burial history, composition of the organic matter (OM) and ultimately the

* Corresponding author.
E-mail address: je136@le.ac.uk (J.F. Emmings).

http://dx.doi.org/10.1016/j.chemgeo.2017.09.012
Received 13 February 2017; Received in revised form 10 August 2017; Accepted 10 September 2017
Available online 21 September 2017

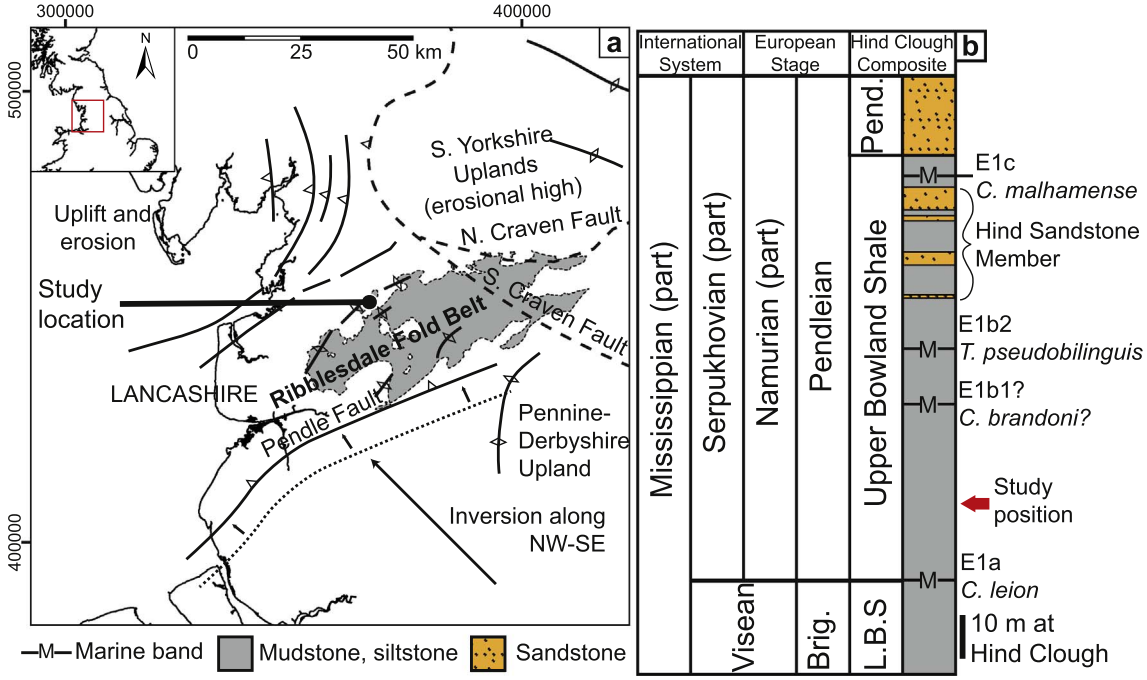

Fig. 1. (a) The Ribblesdale Fold Belt exposes part of the Craven Basin, including the Bowland Shale Formation at outcrop locality Hind Clough (Brandon et al., 1998). Main Westphalian structural elements are also provided (after Fraser and Gawthorpe, 2003). Outcrop extent data are based on DigiMapGB-625, published with permission of the British Geological Survey. British National Grid projection. (b) Craven Basin stratigraphy, Hind Clough (after Brandon et al., 1998; Menning et al., 2006; Waters et al., 2007). Brig. = Brigantian, Arns. = Arnbergian L.B.S = Lower Bowland Shale, Pen. = Pendleton Formation.

timing of hydrocarbon generation between basins. Analysis of outcrop samples can greatly improve the understanding of processes that operated within the Craven Basin to address these uncertainties, but only on the basis that fresh, unweathered samples are available. We delineate the effect of weathering in a temperate climate and assess the nature of weathered zones using a suite of short hand-held drill core samples of the Bowland Shale. We present a suite of Rock-Eval pyrolysis, carbon isotope compositions of OM ($\delta^{13}C_{org}$) and inorganic geochemical data typically used in the characterisation of hydrocarbon source rocks.

1.1. Controls on weathering of organic-rich mudstone

It is often assumed that relatively fresh outcrop samples may be acquired from the outcrop slope if 'dug out' from beneath the weathered surface zone (e.g., Littke et al., 1991; Tuttle et al., 2009). However, beyond visual inspection at the outcrop, it is difficult to rapidly assess whether samples are altered due to modern weathering and to estimate the thickness of the weathered zone. Weathering zones develop in response to specific physical and chemical conditions, driven by climate (for example tropical, humid, semi-arid or arctic climatic zones), including vegetation type (e.g., depth of the rhizosphere and water table; Leythaeuser, 1973), and the nature of the protolith.

The protolith may exhibit variable lithology, bulk density, inclination of beds, joints, and fractures, and exposure aspect, for example (e.g., Leythaeuser, 1973). The original concentration of redox sensitive components, such as OM and sulphides (e.g., 'black' and 'grey' shale), also results in differing rates of weathering through buffering and/or enhancement of weathering (e.g., by development of organic porosity; e.g., Petsch, 2014). The oxidation of these components is therefore a proxy for weathering (e.g., Wildman et al., 2004). Sulphides are considered to be a more useful proxy for weathering than OM because they are a faster electron donor during weathering (Petsch et al., 2000). Since the efficiency of weathering may be highly variable, the thickness of weathering zones varies from several centimetres (e.g., Fischer and Gaupp, 2005), decimetres (e.g., Clayton and Swetland, 1977) to metres (e.g., Tuttle et al., 2009).

Another consideration is whether exposures occur in weathered slopes or stream-cut sections. Away from coastal sections, stream-cut sections are preferred over slope sections. This is because perennial streams are thought to expose unweathered material at the outcrop surface, since the rate of physical erosion by bedrock abrasion is typically greater than the rate of chemical alteration (Small et al., 2015). Yet the assumption that fresh material can be acquired from streams has not been tested.

In this study, samples from two stratigraphically equivalent levels, a perennial stream and an adjacent weathered slope section are compared. We show that the perennial stream exposes fresh mudstone at the outcrop surface, because the rate of bedload abrasion is likely greater than the rate of chemical alteration. Natural fractures are a conduit for oxidising meteoric waters that promote leaching of mudstone adjacent to fractures, but these layers can typically be avoided during sampling or removed during laboratory sample preparation. Weathering on the slope generates bedding-parallel fractures that exploit heterogeneity in the initial sedimentary fabric. Along bedding-parallel fractures, millimetre- to centimetre-scale leached layers and iron oxide coatings are common. We demonstrate *in situ* material recovered from the surface of the weathered slope adjacent to the stream is not the most chemically altered, however, probably because physical weathering processes here dominate over chemical processes at the surface. The most chemically altered mudstone on weathered slopes is found several tens of centimetres into the outcrop, where the rate of chemical alteration is greater than the rate of physical weathering. Material sampled at the surface of the slope is chemically unaltered but potentially represents a biased record driven by the non-random development of fractures associated with initial sedimentary fabric heterogeneity (such as laminae).

2. Geological setting

The outcrop locality, Hind Clough (grid ref: 364430 453210, British National Grid projection), exposes a 124 m thick succession of

Mississippian Bowland Shale Formation, located within the Bowland sub-basin of the Craven Basin (e.g., Brandon et al., 1998; Fraser and Gawthorpe, 2003; Fig. 1a). The Craven Basin formed part of a series of extensional, epicontinental basins that linked a seaway between present-day North America to the Lublin Basin, Poland (Guion et al., 2000). Extension, then later thermal subsidence, provided accommodation for the deposition of dominantly argillaceous syn-rift sediments that interdigitate with (and were progressively onlapped by) fluviodeltaic sediments derived primarily from the north and north-east (Hallsworth et al., 2000; Waters and Davies, 2006). Variscan inversion of the Craven Basin, primarily during the Pennsylvanian (Westphalian), resulted in the development of a set of north-east south-west trending folds, thrust-folds and monoclines. These structures are collectively defined as the Ribblesdale Fold Belt (Arthurton, 1984; Gawthorpe, 1987), which have resulted in several surface exposures of the Bowland Shale, including at Hind Clough.

The identification of 'marine bands' (glacioeustatic flooding surfaces; e.g., Ramsbottom, 1977; Davies, 2008), containing diagnostic faunal (ammonoid) assemblages, permits correlation across the Craven Basin and in some instances across several basins (Ramsbottom and Saunders, 1985; Waters and Condon, 2012). From the Lower Bowland Shale (P2c ammonoid zone) to the base of the Pendleton Formation (cutting into E1c ammonoid zone), the dominant mudstone lithology is exposed almost continuously within a perennial stream section and adjacent slope exposure (Fig. 1b). Mudstones are interbedded with carbonate-cemented siltstones to fine sandstones. The stream begins at a series of springs within the interbedded Hind Sandstone Member and Bowland Shale mudstones (Fig. 1). The upstream extent of the stream is therefore limited to the Bowland Shale, Hind Sandstone, nearby soils and glacial sediments within the catchment. The Pendleton Formation (overlying the Bowland Shale) caps the hilltop.

3. Materials and methods

The outcrop site was selected based on quality of exposure and the identification of marine band marker horizons, including key nektopelagic (ammonoid) macrofauna, to enable correlation with deep borehole core data and other outcrop sites. Outcrop cores were located within the E1a biostratigraphic zone, at two stratigraphic positions, 12 m and 16 m above the base of the E1a (*Cravenoceras leion*) marine band (Fig. 1b).

Sampling was conducted with a hand-held drill which penetrated to a maximum of 1.25 m into the outcrop with complete recovery of core (Fig. 2a). A 51 mm outer diameter core bit (~47 mm inner diameter) was used in order to acquire sufficient material across a small stratigraphic interval in each core. Stream water was used as the drilling fluid. The stratigraphic position of drill cores and any overlap between cores was estimated in the field using the dip and strike of bedding with an Abney level. Bed dip is typically < 5°, towards the SW. The drill cored directly into in situ mudstone; loose material was absent at the selected coring positions. Further onto the slope (i.e., between cores 1A/1B/4 and 3/5), patchy accumulations of several centimetres to tens of centimetres of mudstone scree are present on top of the outcrop (Fig. 2a).

Two intervals were sampled. A lower stratigraphic interval was drilled, from which cores (DC) 1A, 1B (stream) and 3 (slope) were obtained. An upper stratigraphic interval was drilled and the cores labelled DC4 (stream) and DC5 (slope). These two intervals demonstrate the contrasting response to weathering; the lower stratigraphic interval is more fissile than the upper stratigraphic interval. DC1A, DC1B and DC4 were oriented perpendicular to bedding. DC1B overlaps with the lower part of DC1A and provides a comparison at the same horizon cored at the stream surface (1B) with 1 m below the stream bed (1A). Slope drill cores DC3 and DC5 were oriented parallel to bedding to minimise mineralogical/geochemical variations that might relate to stratigraphic changes and to investigate the lateral distribution of OM.

Core samples were described on a centimetre scale and logged to engineering geological standards (BS 5930:1999), including bulk weathering characteristics (including designation of weathering grades; Table 1). A second phase of sedimentological logging recorded changes in lithology, grain size and sedimentary structures including, for example, the presence of macroscopic OM and bioclastic debris. The subsampling strategy focussed on understanding possible bulk changes in the organic and inorganic composition along each drill core in relation to the observed weathering grades (Section 4.1). Lithobiontic coatings such as lichen, fungi and algae were not evident (e.g., Dorn, 2013), therefore are not considered to contribute significantly to the bulk geochemical analyses.

Data collected from G-BASE stream and sediment sample no. 353130 (Johnson et al., 2005), positioned 500 m downstream of the study site (grid ref: 364640 453860), were used for comparison and consideration of the downstream fate of elements. The G-BASE sediment sample was collected from the active stream channel, wet sieved and analysed for major and trace element concentrations. Stream water alkalinity, pH and conductivity were determined on location (see Johnson et al., 2005).

3.1. Analytical methods

Eighteen pairs of homogenised powdered subsamples were selected for inorganic and organic analyses. Whole-rock powder and clay fraction XRD data were collected on a Bruker D8 Advance Powder Diffractometer equipped with a LynxEye Position Sensitive Detector with a Bragg Brentano, flat plate θ-θ geometry using CuKα radiation. Clay-fraction XRD data for one sample were interpreted in accordance with the method defined by Poppe et al. (2001). Scanning electron microscopy (SEM) was conducted on uncoated thin sections using an S-3600 N Hitachi microscope with Oxford INCA 350 EDS used for elemental mapping. Total carbon (TC) and total sulphur (TS) were determined by analysis using a LECO CS 230 elemental analyser. XRF data were acquired on fused beads and powder briquettes with a PANalytical Axios Advanced X-Ray Fluorescence spectrometer using default PANalytical SuperQ conditions. Major and trace elements in the G-BASE stream sample were also determined using XRF (Johnson et al., 2005).

Pyrolysis was conducted on finely powdered samples in a Rock-Eval 6™ apparatus (Vinci Technologies) at the British Geological Survey. Data generated include total organic carbon (TOC), hydrogen index (HI) and oxygen index (OI). $\delta^{13}C_{org}$ analysis was determined on both untreated and decarbonated powders by combustion in a Costech ECS4010 elemental analyser. Reported $\delta^{13}C_{org}$ values are on the VPDB scale, based on the analysis of reference materials calibrated to NBS18, NBS19, and NBS22. Two additional pyrolysis and $\delta^{13}C_{org}$ analyses were conducted on samples 'coupled' with another sample at the same stratigraphic position; samples 2 and 3 (grade II-B and I) and samples 4A and 4B (grade I and II-A). A full description of methods used, including estimates for accuracy and precision, is provided in Appendix I.

3.2. Principal components analysis

A principal components analysis (PCA) was conducted using R (R Core Team, 2015) in order to reduce the complexity of the data. Data were scaled and centred but no other transformation was performed. The length of the first axis, generated from a detrended correspondence analysis (Oksanen et al., 2016), was assessed prior to the PCA in order to confirm a linear (rather than unimodal) data distribution. Significance (using *p*-values) of principal component eigenvalues (loadings) for each variable, considering loadings on both PC1 and PC2, was estimated using a permutation resampling method designed to account for data with latent variables driven by lithology (Chung et al., 2015; Chung and Storey, 2015). The total number of principal components included in the significance test was determined by assuming a cut-off at the 'elbow' in the respective scree plot for eigenvalue plotted against

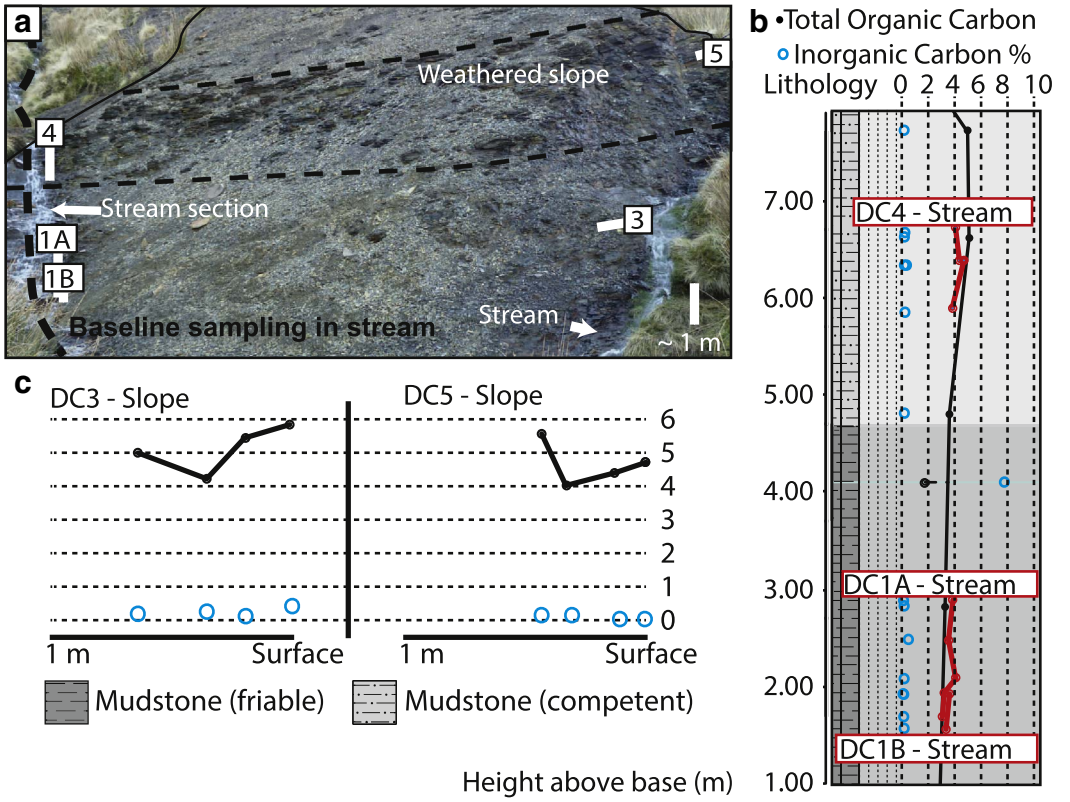

Fig. 2. (a) Field photograph indicating positions of drill cores. (b) Sedimentary log through part of the section with total organic carbon (TOC, wt%) and inorganic carbon (wt%) from RockEval pyrolysis, including 'baseline' samples acquired throughout the section at the stream surface. (c) TOC and inorganic carbon data for slope cores.

Table 1
Definition of weathering grades.

Grade	Description	Setting	Interpretation
I	Competent, visually unaltered material (lack of alteration halos or fissile texture)	Stream	Unweathered, fresh material
II-A	< 1 mm thick alteration halos in the vicinity of natural fractures; material is otherwise visually unaltered	Stream & slope	Oxidation of pyrite along tight natural fracture surfaces; limited penetration
II-B	> 1–2 mm thick alteration; sample is completely altered based on visual inspection	Stream & slope	Oxidation of pyrite along natural fracture surfaces
III-A	< 1 mm thick alteration halos along bedding fractures; material is otherwise visually unaltered	Slope	Mechanical weathering along planes of weakness; oxidation of pyrite within layers along bedding planes
III-B	~1–2 mm thick alteration halos along bedding fractures; material is otherwise visually unaltered	Slope	Mechanical weathering along planes of weakness; oxidation of pyrite within layers along bedding planes
III-C	> 2 mm thick alteration halos along bedding fractures; material is extremely fissile	Slope	Mechanical weathering along planes of weakness, fractures are relatively open and surfaces are characterised by extensive oxidation of pyrite within layers along bedding planes
IV	Fissile 'paper shale' texture; material is otherwise visually unaltered with the exception of patchy alteration halos at the outcrop edge	Slope, DC5 only	Mechanical weathering along planes of weakness; the rate of mechanical weathering is ≫ chemical alteration

Modifiers: I = unweathered, II = sub-vertical fractures, III = bedding fractures, IV = paper shale.

component.

68% confidence ellipses were generated for each sample using a bootstrap approach (Canty, 2002) with 1000 resample iterations (Starmer, 2015). This method provides a qualitative test for the stability of the principal components plot and to consider the reliability of any clustering. Major element XRF data is 'closed', so that concentrations sum to 100%. Thus interpretation of the PCA considers that any observed inverse relationships in these data, such as between Si and Al, for example, is likely a result of the changing the degree of Si dilution (i.e., this can be interpreted as a lithological difference only).

4. Results

4.1. Weathering grades

Macroscopic observations differentiate seven weathering grades (Table 1; Fig. 3). These grades are not mutually exclusive and form part of a continuum from the visually fresh mudstone (grade I) end-member to the physically weathered 'paper shale' end-member (grade IV).

Grade I mudstone is observed only in stream cores (1A, 1B, 4) as visually unaltered, competent, blocky to flaggy mudstone (Fig. 3b). The occurrence of altered zones (typically up to 2 mm thick) on sub-vertical 'natural' fractures defines grade II alteration. II-A defines material with alteration zones that are relatively thin (< 1 mm thick). II-B defines

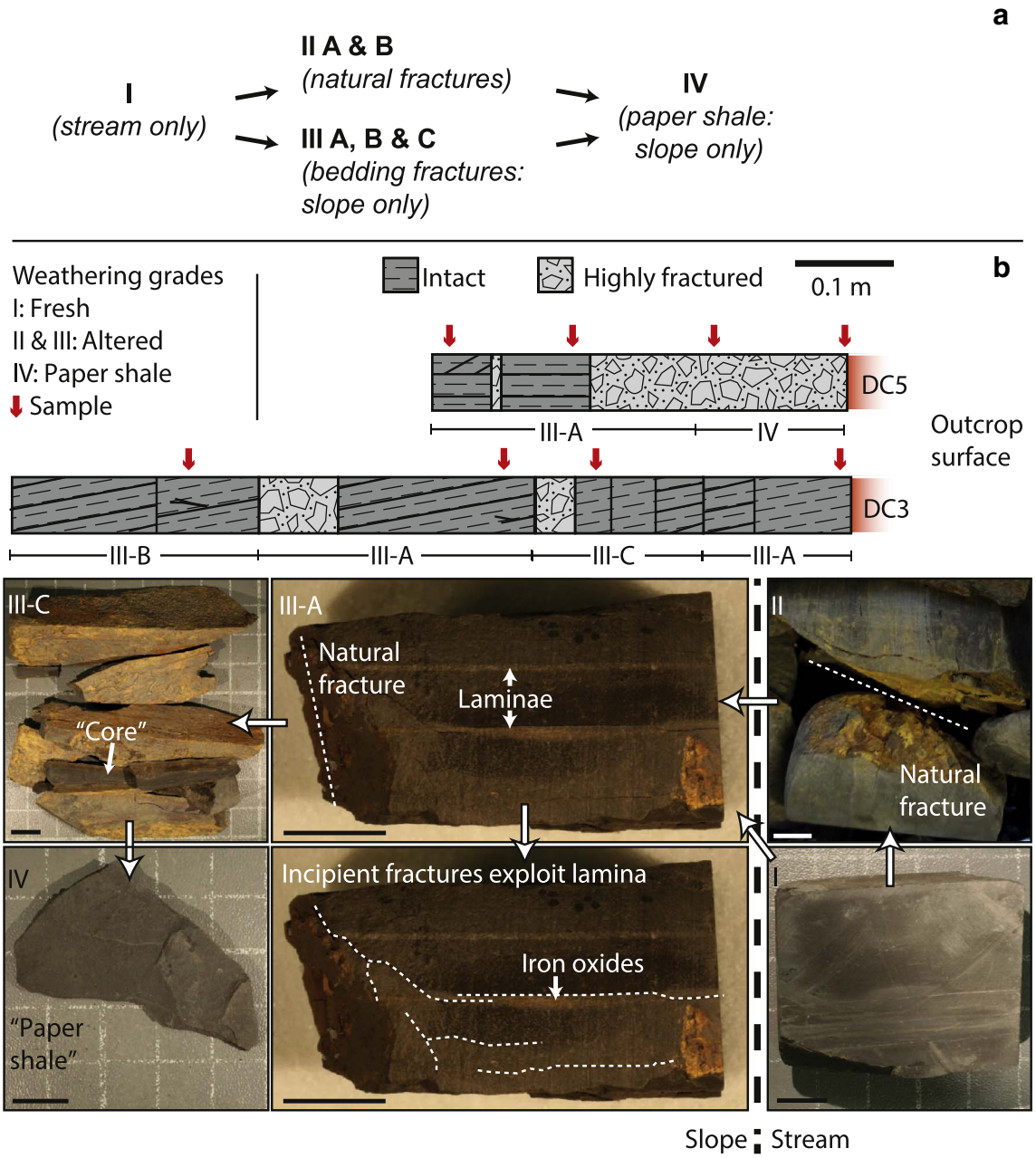

Fig. 3. Weathering grades. (a) Weathering flow diagram. (b) Sample positions (slope cores only) and example photographs for weathering grades. Scale bar in photographs is 10 mm.

material with alteration zones thicker than 1 mm. Natural fractures are typically spaced 0.1 to 0.3 m apart. Alteration zones that occur along bedding-parallel (herein 'bedding'), rather than 'natural', fractures are termed III-A, III-B and III-C depending whether alteration zones are thinner than 1 mm or thicker than 5 mm. Bedding fractures are absent within the stream section. Altered surfaces are far more common on the weathered slope. Grade IV mudstone, observed only on the upper slope at DC5, is characterised as a well-developed fissile texture often termed 'paper shale' (e.g., Dyni, 2006). Most exposed surfaces appear unaltered, but with increasing depth into the outcrop, fracture surfaces become altered; the boundary between IV and III material within the outcrop is sharp, at 0.15 m below the outcrop surface. The absence of grade IV material in DC3 may relate to close proximity to a stream that cuts the base of slope (Fig. 2).

4.2. Mineralogy and inorganic geochemistry

Whole-rock and clay-fraction XRD analysis indicate a composition of quartz, pyrite and a mixture of kaolinite and illite clay minerals for grade I material. Trace calcium carbonate (calcite) is present in all samples. Plotting Si/Al and (Na + K)/Al (Fig. 4a; Velde and Meunier, 1987) corroborates the XRD data that quartz (plus biogenic silica) and illite dominate the mineralogy, with minor kaolinite. Samples plot on a continuum towards higher Si/Al, interpreted to indicate a greater abundance of quartz and/or biogenic silica compared to illite and kaolinite. Mineral carbon content from pyrolysis indicates all samples contain a broadly similar trace carbonate content of 0.17% (± 0.18%, 2σ, n = 19). Plotting Fe and S (Fig. 4b) indicates that grade I samples plot on a continuum along S/Fe ~1.10.

In thin section, the sedimentary fabric for grade I samples is characterised by an abundance of silt to sand-sized mud lenses within a clay-sized matrix (Fig. 5a–c). This fabric is punctuated by widely spaced

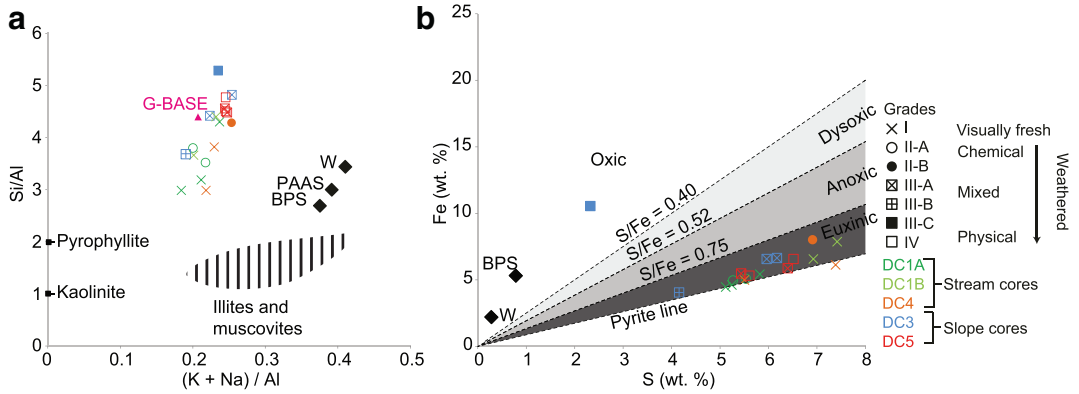

Fig. 4. (a) Molecular alkali (K + Na)/Al and Si/Al plot. PAAS = Post-Archaean Shale Composite (Taylor and McLennan, 1985), BPS = British Lower Palaeozoic Shale (Plant and Jones, 1989), W = average shale (Wedepohl, 1995). End-member mineral compositions are plotted for comparison (from Norry et al., 1994). G-BASE site stream (particulate fraction) data plotted only as K/Al, from Johnson et al. (2005). G-BASE data reproduced with the permission of the British Geological Survey ©NERC. All rights Reserved. (b) Total Fe versus S, including BPS (Plant and Jones, 1989) and W (Wedepohl, 1995) data. S/Fe fields are plotted using data from Raiswell et al. (1988). If all Fe and S are assumed to be sulphidic, the data plot in the 'euxinic' field. Some Fe may be present in detrital and unreactive minerals (e.g., silicates). The grade III-C sample plots with low S/Fe in the 'oxic' field.

laminae (typically spaced 15 mm apart, 1 to 5 mm thick) with a variety of compositions including silt-sized grains and clay-rich layers that do not contain lenses. Three zones (Z1, Z2, Z3) of increasing alteration intensity are observed in thin section. Grade II and grade III samples exhibit Z1 alteration, which is readily observed in thin section. The sedimentary fabric is continuous from unaltered material into each altered Z1 zone (Fig. 5b). Strong electron backscattering under SEM primarily delineates pyrite framboids, which are absent within Z1 alteration zones (Fig. 5c). Fe element maps, and Fe and S element maps, are used as a proxy for iron oxides and pyrite, respectively. The absence of these elements in Z1 altered zones corroborate the backscatter data that indicates an absence of pyrite within alteration zones for grade II samples (Fig. 5d, e). Carbon is relatively enriched in the Z1 alteration zone (Fig. 5f).

The grade III samples are on a continuum, from minor to extensive alteration. Alteration is zonal and often concentric (for III-B and III-C) because it occurs along parallel bedding fractures. An inner 'core' of unaltered grade I material is surrounded first by Z1 alteration zones (Fig. 5g–o). A second alteration zone, Z2, is characterised by gradual increases in the abundance of Fe towards the Z3 zone. The contacts between Z1 and Z2, and Z2 and Z3, are sharp. Z3 zones comprise the iron oxide goethite (based on optical microscopy and XRD). This is corroborated by relatively high abundances of Fe in the Z3 zones, which track along both natural and weathering fracture surfaces and truncate the sedimentary fabric (Fig. 5j, m).

Weathered slope samples (including grades III and IV) at both stratigraphic levels exhibit higher Si/Al than unweathered material (Fig. 4a). Deviation from S/Fe ~1.10, as defined by unweathered samples, clearly differentiates the III-C sample, which exhibits low S/Fe and contains goethite alteration coatings (Fig. 5j, m). Grade IV S/Fe plots with grade I material (Fig. 4b). The PCA demonstrates that the compositional variance of grade I and grade IV samples is well defined (Fig. 6a). The grade II-B sample plots together with slightly altered grade II-A samples in poorly defined and strongly overlapping clusters (Fig. 6b), whereas the grade III-C sample plots in a separate cluster with strong covariance with Fe and inverse covariance with S (Fig. 6b). A grade III-A sample also plots in a separate cluster associated with carbonates; this is corroborated by a higher carbonate content than most other samples (Table 2).

Comparison across all major and trace elements (Table 2) indicates the composition of grade III-C and IV samples deviates from the mean grade I composition (Fig. 7a). Element concentrations in the grade II-B sample typically exhibit little deviation from the mean, with the exception of a greater As concentration. Grade II-B and III-A samples also exhibit higher Cu concentration compared to grade I samples. The grade III-C sample exhibits greater concentrations of Fe, P, Pb and Zn and lower concentrations of S, Co, Ni and Ca when compared with grade I samples. Trace element abundances in grade IV samples are typically depleted compared to mean grade I samples.

Normalisation to the TC content (here equivalent to TOC since carbonate is present as a trace component) adjusts for elements primarily contained within OM (e.g., Georgiev et al., 2012; Fig. 7b) and demonstrates similar changes relative to unweathered material. The relative enrichment of Cu and Mo for the grade III-B sample is reduced when normalised to the TC. Use of enrichment factors (Amundson, 2005), using Zr as the index phase, also delineates the same divergences from the unweathered mean (Fig. 7c). Element concentrations for the grade II-B sample are typically depleted relative to mean grade I material (e.g., Cs), although As and Cu remain relatively enriched.

The G-BASE stream particulate sample exhibits enrichment in P, Zn, Mn, Zr, Ba and Al compared to the grade I samples. Conversely, the G-BASE sample exhibits substantial depletion in Mo and slight depletion in As, Cu, Ni, Sb, Sr and U. A value of pH 4 was reported for the stream water.

4.3. Organic matter

Two coupled samples compare grade I with grade II-A, and grade I with II-B material, at the same depth in DC4 (at 0.42 m below surface). Comparison between grade I and II-A samples is uncertain because differences are within the analytical error. However, compositional differences between grade I and II-B are notable; S1 decreases by 0.6 mgHC/g rock and S2 decreases by 3.2 mgHC/g rock. These relationships are observed for most samples; grade I samples typically exhibit higher S1, higher S2 and lower S3 than grades II and III samples (Table 2; Fig. 8a). Based on these observations, a series of linear relationships were propagated throughout the organic dataset, and enable the estimation of the original organic composition prior to weathering. Altered slope samples are extrapolated back along each curve into the likely zone for unweathered material. This method assumes minimal change in the type of OM between samples. For example, a van Krevelen-style plot for HI and OI (Fig. 8b) indicates that grade II and III samples exhibit lower HI and higher OI than grade I material. HI decreases by 58 mgHC/gTOC, and OI increases by 19 mgCO + CO_2/gTOC, between the coupled grade I and II-B samples. Chemically altered samples are then extrapolated back into the unweathered field along HI = (− 3.00 × OI) + 181. Grade IV samples plot together with grade I samples in the unweathered zone for all Rock-Eval parameters.

TOC content ranges between 3 and 5 wt% for grade I samples and exhibits an exponential relationship with HI (Fig. 2; Fig. 8c), similar to

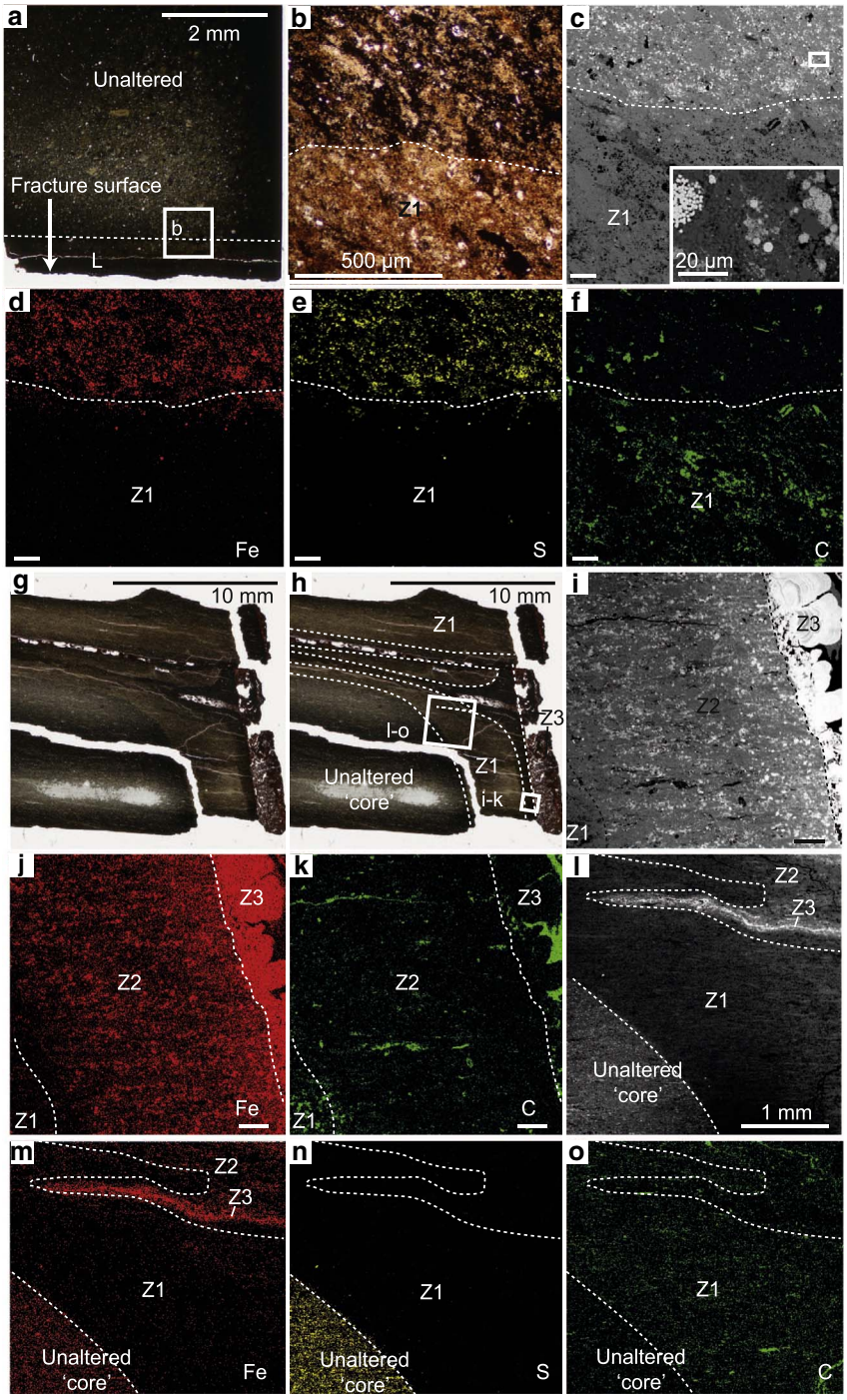

Fig. 5. (a)–(f) Grade II (A and B) alteration features. (g)–(o) Grade III-C alteration features. (a) Thin section scan, perpendicular to a sub-vertical fracture surface. A thin grade II alteration surface is present parallel to the fracture. (b) Thin section microphotograph, demonstrates the majority of opaque minerals, sulphides, are absent within the grade II alteration zone. (c) Backscattered electron (BSE) microphotograph reveals sulphides, primarily pyrite framboids, are absent within the alteration zone. (d)–(f) Relative abundance element maps for Fe, S and C. (g)–(h) Thin section scan, perpendicular to bedding. (i)–(k) BSE microphotograph, Fe and C element maps delineate several zones with an increasing abundance of Fe in the vicinity of a natural fracture. S was below the limit of detection. (l)-(o) BSE microphotograph, Fe, S and C element maps delineate a core of unaltered (grade I) material, followed by a progressive increase in the abundance of Fe in the vicinity of incipient fractures. Z1 = zones with an absence of pyrite. Z2 = zone of moderate Fe concentration. Z3 = zone of high Fe concentration. Scale bars are 100 μm unless stated.

other organic-rich mudstones (e.g. Dean et al., 1986; Deroo et al., 1980; Deroo et al., 1983; Herbin et al., 1983; and Tyson, 1995). Comparison with other data is treated with caution, however, due to differences in organic composition and maturity. Grade II and III samples deviate towards lower HI and TOC than grade I and grade IV material; for example the coupled grade I and grade II-B samples exhibit difference of 0.34 wt% TOC. $\delta^{13}C_{org}$, used as a proxy for the type of OM (Davies et al., 2012), ranges between −26.5 and −29.0‰ for grade I and grade III samples (Fig. 8d). The coupled grade II-B sample exhibits more positive $\delta^{13}C$ than the grade I counterpart with a 0.1‰ difference (although this is very close to the analytical error). The grade II-B sample also contains less pyrolizeable carbon than the grade I counterpart and the grade IV samples (Fig. 8e, f). The mean T_{max} for all samples is 431 °C (± 2 °C, 2σ, n = 19). The coupled I with II-B samples recorded T_{max} of 440 °C and 429 °C, respectively.

4.4. Principal components

PCA provides a means to integrate and reduce the complexity of the inorganic and organic data. PCA for unweathered samples (Fig. 6a) is considered to be stable and indicates a series of associations between elements and the Rock-Eval parameters. Considering the first two principal components, Fe, As, Ba, Cr, Pb, Sb, Se, V and Zn exhibit significant loadings. PCA for weathered samples (Fig. 6b) indicates several of the relationships between elements are disrupted (with the exception of Th, Pb and Zn). The extensive overlap of PCA confidence ellipses for weathered samples indicates instability and therefore interpretation of Fig. 6b is limited.

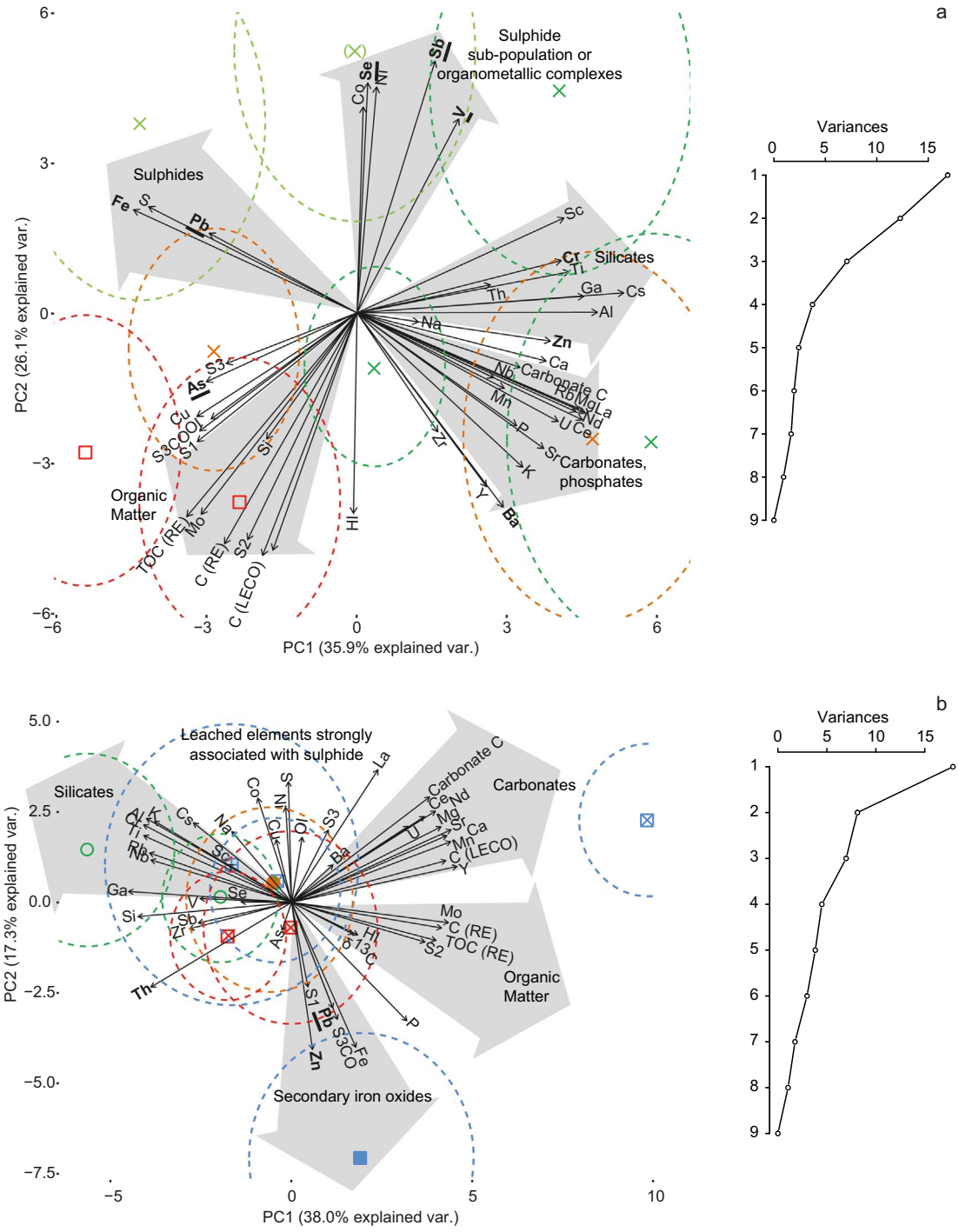

Fig. 6. RockEval pyrolysis parameters plotted with major and trace elements using a classical Principal Components Analysis (PCA) based on a correlation matrix, projected for the first two principal components (PC1, PC2). Underlined and bold variables exhibit loadings considered to be highly significant, with *p*-values below 0.05. Variables in bold only, exhibit loadings considered to be significant, with p-values below 0.10. 68% confidence ellipses are also plotted to provide an indication of the stability of the principal components with respect to sampling variation. (a) Grade I and grade IV samples. Minimal overlap between data points, especially between weathering grades, indicates the PCA is stable. (b) Chemically altered samples (II-A, II-B, III-A, III-B, III-C). Overlap of ellipses indicates significant uncertainty. Legend as in Fig. 4.

5. Discussion

5.1. Chemical processes

Grade I material is found only within the stream-cut section, in direct contact with stream waters (Fig. 2). The composition of grade I samples includes a variety of elements that indicate deposition under reducing conditions. For example, S/Fe for grade I samples plot within a field that represents 'euxinic' conditions during deposition (Raiswell et al., 1988), if it is assumed that all S and Fe is pyritic for unweathered samples (Lyons and Severmann, 2006). Enrichment in redox sensitive trace elements (e.g., Mo, U, V, Cu, Ni; e.g., Tribovillard et al., 2006) also indicates deposition under anoxic or euxinic conditions. Since a reduced signal is preserved by grade I samples, oxidative chemical weathering is readily identified.

5.1.1. Natural fractures

Pyrite is absent in Z1 alteration zones parallel to sub-vertical natural

Table 2
Selected results.

Grade	Sample/ core	Major elements (wt%)										LECO (wt%)		LOI
		Si	Ti	Al	Fe	Mn	Mg	Ca	Na	K	P	C	S	
I	1/4	25.43	0.24	6.63	6.18	0.01	0.37	0.02	0.14	1.37	0.03	4.31	7.35	44
	9/1A	24.88	0.29	7.76	4.49	0.02	0.72	0.81	0.11	1.52	0.06	4.18	5.09	46
	10/1A	30.24	0.27	7.00	5.45	0.01	0.51	0.34	0.18	1.47	0.04	3.94	5.82	45
	13/1B	25.30	0.22	5.73	7.93	0.01	0.35	0.04	0.11	1.21	0.02	3.53	7.38	44
	14/1B	27.94	0.32	7.60	6.53	0.01	0.43	0.14	0.15	1.37	0.02	3.52	6.92	45
	11/1A	25.31	0.35	8.43	4.67	0.01	0.44	0.16	0.11	1.43	0.02	3.22	5.24	46
I#	4B/4	28.07	0.36	9.36	5.07	0.01	0.56	0.13	0.16	1.87	0.03	4.00	5.47	46
II-A	8/1A	30.09	0.30	7.91	5.13	0.01	0.42	0.03	0.09	1.48	0.02	3.83	5.52	46
	12/1A	29.76	0.33	8.43	5.01	0.01	0.49	0.16	0.16	1.66	0.02	3.17	5.25	46
II-B*	2/4	28.37	0.25	6.62	8.06	0.01	0.44	0.11	0.16	1.51	0.05	4.85	6.87	44
III-A	7/5	30.51	0.27	6.68	5.49	0.01	0.40	0.01	0.09	1.53	0.02	4.80	5.40	45
	15/3	25.78	0.21	5.34	6.57	0.03	1.56	2.72	0.11	1.24	0.08	6.66	5.94	44
	6/5	29.89	0.27	6.66	5.92	0.01	0.40	0.02	0.11	1.53	0.02	5.22	6.37	44
	18/3	29.40	0.26	6.62	6.66	0.01	0.38	0.05	0.14	1.33	0.04	4.99	6.10	45
III-B	17/3	30.45	0.33	8.22	4.07	0.01	0.43	0.12	0.11	1.44	0.02	4.34	4.13	47
III-C	16/3	28.78	0.23	5.44	10.58	0.01	0.33	0.01	0.09	1.18	0.12	4.20	2.29	47
IV	5A/5	29.89	0.26	6.24	6.63	0.01	0.38	0.01	0.10	1.42	0.02	4.56	6.49	45
	5B/5	30.62	0.27	6.77	5.33	0.01	0.42	0.01	0.12	1.53	0.02	4.91	5.58	45
Mean I	–	26.74	0.29	7.50	5.76	0.01	0.48	0.23	0.14	1.46	0.03	3.81	6.18	45
I*	3/4	–	–	–	–	–	–	–	–	–	–	–	–	–
II-A#	4A/4	–	–	–	–	–	–	–	–	–	–	–	–	–
G-BASE 353130		66.62	0.71	15.19	12.58	0.35	0.92	0.53	–	3.14	0.35	–	–	–

Grade	Trace elements (ppm)														Rock-Eval pyrolysis									$\delta^{13}C_{org}$
	As	Co	Cs	Cu	Mo	Ni	Pb	Sb	Sc	Se	U	V	Zn	Zr	S1	S2	S3	S3CO	TOC	OI	HI	MinC	T_{max}	
I	202	39	15	72	72	145	250	12	16	17	19	144	39	77	1.58	5.96	0.13	0.11	4.10	3	145	0.14	427	−28.1
	54	31	23	77	50	121	154	13	15	9	20	138	95	68	1.10	5.27	0.02	0.02	3.56	1	148	0.53	432	−27.9
	71	30	16	71	60	128	193	15	15	17	20	165	128	64	1.44	6.23	0.02	0.02	4.11	1	152	0.18	432	−28.1
	133	42	15	83	57	148	264	18	12	20	11	134	37	58	1.51	4.85	0.02	0.02	3.64	1	133	0.11	426	−27.6
	106	34	16	85	46	153	225	22	15	43	16	235	33	69	0.61	3.37	0.03	0.03	3.37	1	100	0.17	436	−26.6
	100	40	21	73	38	137	178	27	19	44	20	299	91	77	0.72	4.65	0.01	0.01	3.23	0	144	0.13	438	−27.4
I#	161	31	22	70	69	110	213	8	18	11	27	142	82	93	0.98	5.34	0.00	0.04	3.84	1	139	0.13	429	−28.1
II-A	68	29	19	96	52	96	218	12	10	12	21	116	91	65	1.26	5.58	0.00	0.03	3.90	1	143	0.14	434	−27.8
	70	31	18	105	40	128	204	19	14	45	17	326	39	70	0.98	4.12	0.00	0.14	3.09	5	134	0.15	428	−28.6
II-B*	225	33	14	113	78	108	294	10	14	27	18	168	52	74	0.97	4.67	1.10	0.14	4.39	25	106	0.23	440	−28.7
III-A	62	24	10	141	68	87	137	8	10	18	15	158	33	79	0.75	9.35	0.47	0.17	5.55	11	168	0.18	440	−28.6
	69	27	13	117	104	116	217	8	10	22	28	131	44	57	1.08	9.20	0.64	0.18	5.83	11	158	0.42	430	−28.7
	127	26	14	161	73	90	135	8	9	18	15	159	35	80	1.47	5.78	0.00	0.24	4.01	6	144	0.14	429	−28.5
	83	47	13	107	82	153	209	12	14	21	15	167	83	63	0.57	5.21	0.47	0.10	4.21	11	124	0.19	441	−28.0
III-B	41	22	16	170	49	61	111	8	11	13	12	121	27	73	0.56	4.61	1.51	0.20	4.98	30	93	0.27	442	−28.5
III-C	95	10	11	95	77	51	328	12	10	24	13	167	145	68	1.30	7.53	0.16	0.34	5.43	6	139	0.12	423	−28.7
IV	154	27	12	119	77	95	175	7	9	18	14	128	31	77	1.27	6.93	0.04	0.09	4.74	3	146	0.10	426	−28.7
	171	22	15	124	72	87	228	7	9	16	17	149	31	79	1.35	7.21	0.05	0.05	4.39	1	164	0.10	427	−28.4
Mean I	118	35	18	76	56	135	211	16	16	23	19	178	72	72	1.13	5.10	0.03	0.04	3.69	1	137	0.20	432	−27.7

(*continued on next page*)

Table 2 (*continued*)

Grade	Trace elements (ppm)													Rock-Eval pyrolysis								$\delta^{13}C_{org}$
	As	Co	Cs	Cu	Mo	Ni	Pb	Sb	Sc	Se	U	V	Zn	Zr	S1	S2	S3	S3CO	TOC	OI	HI	MinC	T_{max}	
I*	–	–	–	–	–	–	–	–	–	–	–	–	–	–	1.58	7.78	0.00	0.27	4.73	6	164	0.09	429	− 28.8
II-A#	–	–	–	–	–	–	–	–	–	–	–	–	–	–	0.99	5.86	0.00	0.10	3.85	3	152	0.14	431	− 28.0
G-BASE 353130	63	31	–	65	16	76	242	7	–	–	11	192	253	302	–	–	–	–	–	–	–	–	–	–

Grades: I = unweathered II = subvertical fractures III = bedding fractures IV = 'paper shale'. Major and trace elements are reported on a molecular weight % (O-free) basis, and ppm, respectively. Loss on ignition (LOI, wt%) is the initial LOI + oxide O from each major element oxide minus total carbon (TC) and total sulphur (TS). S1 and S2 are reported as mg HC/g rock, S3 and S3CO are reported as mg CO_2 mg/g rock and mg CO/g rock, respectively. TC, TS, total organic carbon (TOC) and inorganic carbon (MinC) are reported on a wt% basis. T_{max} is reported as °C. $\delta^{13}C_{org}$ is reported on a ‰ basis. * and # 'coupled samples' at the same depth. Data presented are open access (Emmings et al., 2017). G-BASE data reproduced with the permission of the British Geological Survey ©NERC. All rights Reserved. See Johnson et al. (2005) for further details.

fracture surfaces that typify grade II-A and II-B samples, indicating oxidation of this phase. The oxidation of pyrite is a typical feature of a relatively early stage of chemical weathering (e.g., Leythaeuser, 1973). The sedimentary fabric is preserved within alteration zones, indicating that Z1 altered zones are leached (similar to inner 'rinds'; Oguchi, 2013). Pyrite oxidation without replacement by iron oxides is consistent with the net loss of both Fe and S from these zones (Fig. 5b). This is best observed in sample II-B, which exhibits S/Fe similar to unaltered material. In addition, whilst the grade II-B sample appears extensively altered, the leached layers are typically thin and preserve an extensive core of unaltered material (similar to Fig. 5h). An exception is the enrichment of Cu in grade II-A, II-B, III-A and III-B samples, which may relate to stratigraphic variation (e.g., changes in the As and Cu content associated with pyrite in unaltered material) or accumulation in secondary phases (e.g., Tuttle et al., 2009).

5.1.2. Bedding fractures

Significant enrichment in Fe, P, Pb and Zn for the grade III-C sample indicates this contains an additional component; these are Z3 coatings of the secondary iron oxide goethite (Dorn, 2013) that likely precipitated from percolating meteoric waters along fracture surfaces. Z3 goethite coatings surround the Z2 zone, which represents a transition from leached (Z1) and precipitated (Z3) domains (Figs. 5j, 4m). Beneath the goethite coatings, the majority of the grade III-C sample is leached and, although distal to fracture surfaces, a core of unaltered material is present. The zoned character of alteration features is comparable to the black shale polyhedron model of Fischer and Gaupp (2005). Understanding how iron oxide coatings relate to leaching is clearly important as these layers could 'seal' fresh material, preventing further leaching of trace elements.

Differences between alteration along stream and slope fractures may relate to fracture density (see Section 5.2) and/or residence time of ambient meteoric waters. A greater fracture density on the slope increases the surface area available for oxidation of sulphides. This will lower ambient pH and Eh (redox potential) compared to meteoric water in natural fractures above streams, especially if the residence time of meteoric waters on the slope is longer. Meteoric waters that percolate along the slope and along fractures above streams will therefore have differing capacity to mobilise elements and precipitate secondary phases. If precipitated, secondary phases, such as iron oxides, have some capacity to fix elements from solution so that some elements may be concentrated. This process explains the difference between thick leached zones and coatings on the slope (III-C) and presence of leached zones (without coatings) in the stream (grade II-B). Differences in the enrichment of Cu between grade II-A, grade II-B, III-A, III-B and III-C samples, for example, might also be explained through this mechanism (e.g., Robertson, 1989).

Depletion of S, Co and Ni in the grade III-C sample may be interpreted in two ways. Positive covariance between Co, Ni, Sb, Se and V in grade I material is interpreted to indicate these elements are associated with a pyrite sub-population, other sulphide phase or organometallic complexes (Fig. 6a) (Huerta-Diaz and Morse, 1992; Tribovillard et al., 2006). The depletion in S, Co and Ni could be interpreted as the result of the precipitation of iron oxides along fracture surfaces that has effectively diluted the concentration of these sulphidic elements. However, the disproportionate depletion of these elements compared to other elements also likely associated with sulphides (Pb, Sb, V), suggests these are leached following oxidation and cannot be accomodated in iron oxides or another phase. S, Co and Ni are therefore transferred into meteoric waters as an aqueous phase (e.g., Tuttle et al., 2009). If the process of leaching of elements during weathering and hydraulic fracturing are comparable, S, Co and Ni may be expected to pose a potential groundwater contamination risk (e.g., Stuart, 2012). Any S remaining within the leached zone is likely to be bound within organic complexes or secondary sulphate. The wide scatter in normalised Ca data (Fig. 7) is likely due to the low abundance of Ca in all samples.

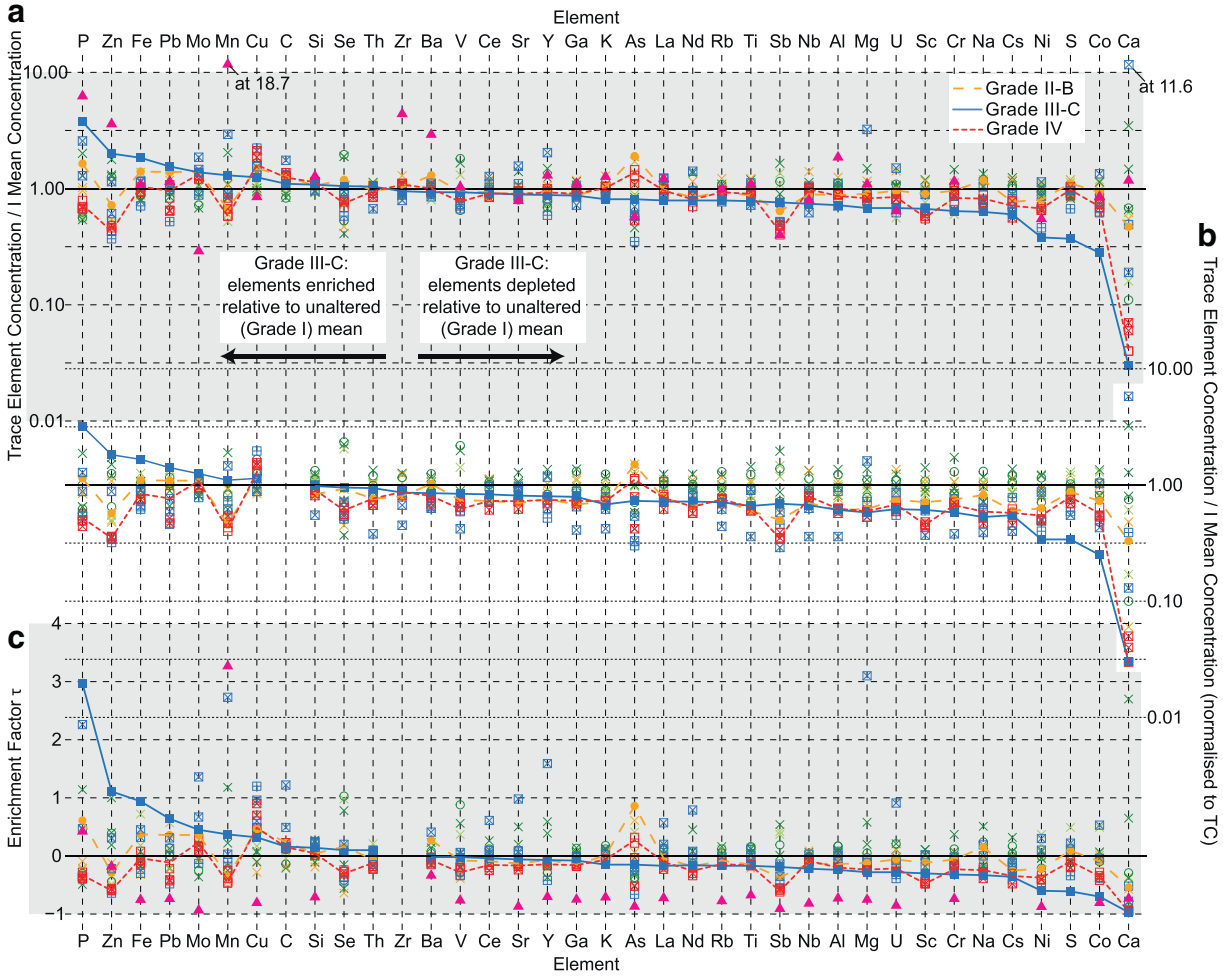

Fig. 7. (a) Major and trace element concentration normalised to the mean grade I mudstone concentration. Elements are ordered from relative enrichment to depletion in the grade III-C sample compared to the grade I (unaltered) mean. (b) Normalised to total C (a proxy for total organic C since carbonates are present in a trace quantity only). (c) Enrichment factors (using Zr as the immobile element) from Amundson (2005). G-BASE particulate fraction downstream elemental analyses at the outcrop are also plotted (triangles), where available (from Johnson et al., 2005). G-BASE data reproduced with the permission of the British Geological Survey ©NERC. All rights Reserved. The mean Zr concentration for grade I samples was used as the index for the G-BASE stream particulate fraction. G-BASE data reproduced with the permission of the British Geological Survey ©NERC. Legend as in Fig. 4.

Despite this, the grade III-C sample exhibits the largest depletion in Ca, which is interpreted as partial dissolution of the trace carbonate phase.

Se can contribute to toxicity (e.g., in farm animals; Fleming and Walsh, 1956), it may be mobile in groundwaters (e.g., Tuttle et al., 2009) and is enriched in the Bowland Shale (Parnell et al., 2016). Se is likely to be associated primarily with a sulphide sub-population (Tuttle et al., 2009) rather than OM (e.g., Mitchell et al., 2012), because it exhibits strong covariance with elements that are primarily accomodated in a sulphide phase. Chemically altered samples exhibit similar concentrations of Se to unaltered samples (Table 2; Fig. 6a) suggesting that it is fixed by secondary iron minerals or clay minerals following pyrite oxidation. Stronger covariance between Se with Al and Si rather than Fe for altered samples (Fig. 6b) suggests Se may be adsorbed by clay minerals (e.g., Peak et al., 2006) rather than iron oxides. This finding indicates that Se is not immediately leached from the outcrop and this places emphasis on the role of mechanical weathering processes (Section 5.2) when considering the fate of Se.

A consistent and positive correlation between Mo concentration and TOC across all weathering grades, including weathered samples, suggests Mo is bound within OM rather than sulphides (e.g., Breward et al., 2015) (Fig. 6a, b). Mo is therefore relatively resistant to oxidation/leaching compared to sulphide-bound trace elements. Conversely, whilst Cu also covaries with TOC (Fig. 6a), this relationship is apparently disrupted for weathered samples (Fig. 6b). This suggests that whilst the enrichment of Mo and Cu are interpreted as indicators for palaeoredox (e.g., Tribovillard et al., 2006), Cu is associated primarily with a sulphide phase rather than with OM, and once oxidised, Cu has accumulated in a secondary phase. Cu enrichment for grade II-A, II-B, III-A and III-B samples, but not the grade III-C sample, suggests Cu is not accomodated within the goethite coatings but instead forms a separate secondary phase or is concentrated by adsorption onto an existing phase within the Z1 leached zones.

5.1.3. G-BASE stream sample comparison

The G-BASE sample provides some indication of the fate of elements either leached from fracture surfaces or transported as particles in the stream following physical weathering. The majority of sediments in the stream are likely sourced locally from the Bowland Shale (Section 3). However, heterogeneity within the Bowland Shale, and the possibility of supply of material from adjacent soils, glacial sediments and from the overlying Pendleton Formation, add uncertainty to interpretations. Stream water composition (e.g., pH) could also be strongly influenced by the input of groundwater. In addition, the role of temporal (e.g., seasonal), hydrodynamic (including possible grain size fractionation) and stream routing (on the scale of metres) effects means only generalised interpretations can be drawn from comparison with the single G-BASE sample.

Elements enriched in the stream sediment compared to

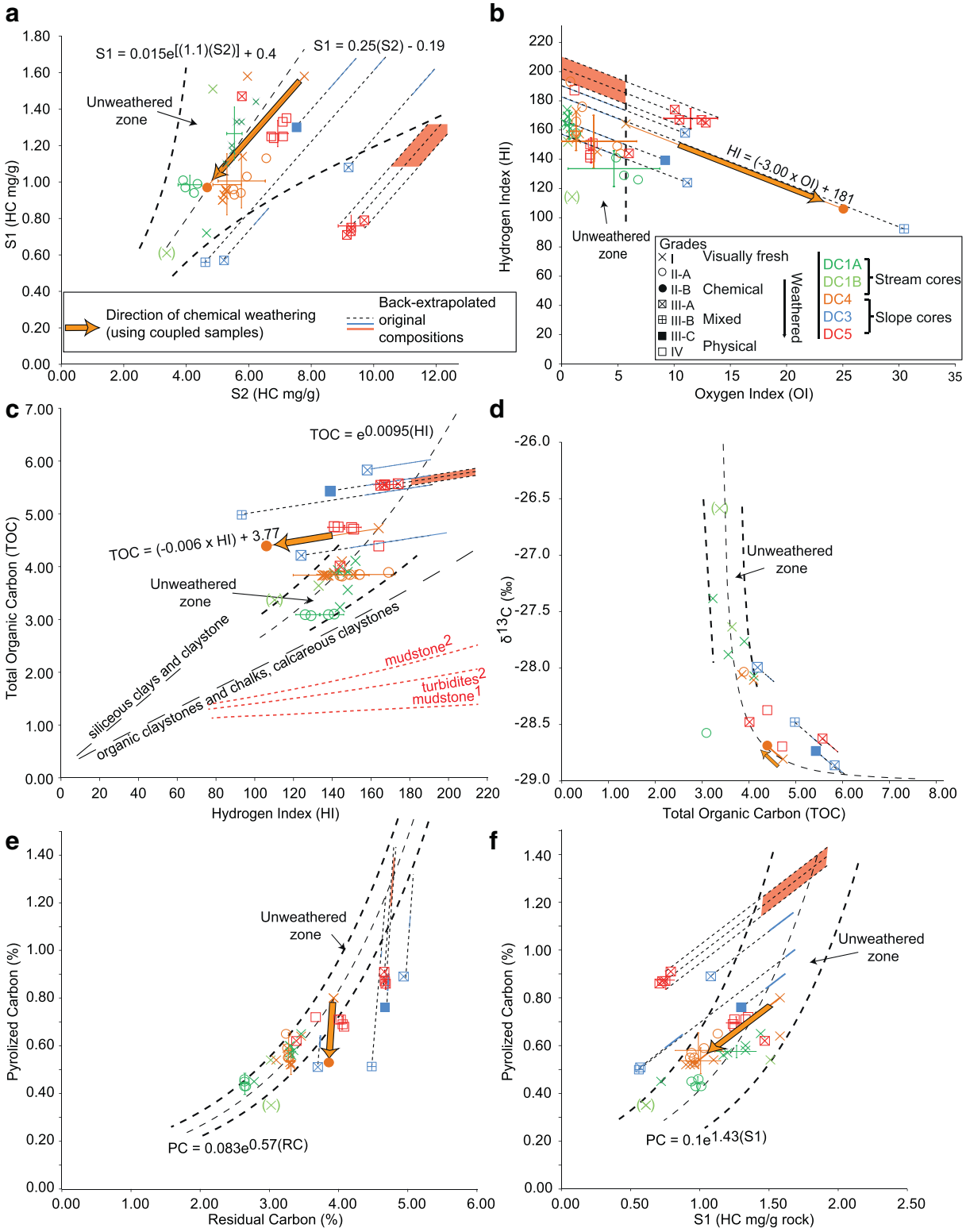

Fig. 8. RockEval pyrolysis parameter comparison for weathering grades. (a) S1 ('free' hydrocarbon) versus S2 ('bound' hydrocarbon) (b) van-Krevelen style plot of hydrogen index (HI) and oxygen index (OI). (c) Total organic carbon (TOC) versus HI. Siliceous clay, chalk and claystone lines based on Cretaceous black shale data from Dean et al. (1986), Deroo et al. (1980), Herbin et al. (1983) and Tyson (1995). Comparison lines for mudstone and turbidites from the Morridge Formation (Bowland Shale equivalent; Waters et al., 2007) from 1) Könitzer et al. (2016) and 2) Gross et al. (2016). (d) $\delta^{13}C_{org}$ versus TOC. (e) Pyrolized carbon versus residual carbon. (f) Pyrolized carbon versus S1. Arrows delineate the effect of chemical weathering. Unweathered fields are estimated based on grade I data. Bracketed grade I sample likely represents sampling of a lamina containing a greater abundance of terrigenous organic matter.

unweathered material (Fig. 7a) are interpreted as relatively immobile, particularly Mn, but also P, Zn, Zr, Ba and Al. Downstream depletion in Mo, and to a lesser degree, As, Cu, Sb, Sr, Ni and U, relative to unweathered material indicates these elements must be either fixed in an intermediate reservoir (e.g. soils, vegetation) between the outcrop and downstream location or that these elements were in solution and

bypassed the G-BASE sample site. If Mo is bound within OM, as the strong covariance with TOC across all weathering grades suggests (Fig. 6a), this indicates most OM travels as a particle in suspension. Downstream bypass would explain low observed concentrations of Mo at the G-BASE sample site. The G-BASE sample analysed particles > 150 μm in diameter (Johnson et al., 2005), therefore it is possible that the stream sediments contain suspended OM (with Mo) but that these particles are smaller than the 150 μm mesh size. The fate of Ni is more difficult to explain because it is not fixed in iron oxides at the outcrop (grade III-C material) nor enriched downstream at the G-BASE sample position. Ni must be transported in solution from the outcrop and locally fixed by vegetation and soils or remains in the aqueous phase. Whilst Co is also leached at the outcrop, the G-BASE sample exhibits a similar Co concentration to unweathered material suggesting Co does not remain in solution downstream.

5.1.4. Alteration of organic matter

Leached zones in both grade II and grade III exhibit changes to the composition of OM, primarily as a decreased HI and increased OI (Fig. 8b) when compared to unaltered material collected from the stream section. This process is interpreted as the accumulation of oxidation products within OM (Petsch et al., 2000), rather than indicating a difference in the original OM composition (e.g., marine or terrestrial origin). Relatively constant $\delta^{13}C_{org}$ across weathering grades also supports the assumption that the type of OM is consistent. Back-extrapolation of grade II alteration along this gradient, where $HI = (-3.00 \times OI) + 181$, into the predicted unweathered field may present a method to estimate original parameters prior to weathering. A similar rate of change for OI/HI between unaltered and weathered samples was observed by Georgiev et al. (2012). Many of the back-calculated original compositional estimates plot within the exepected fields from grade I samples. Whilst S1, OI and OICO parameters co-vary with TOC for grade I samples (Fig. 6a), this relationship is disrupted for weathered samples (Fig. 6b). The best explanation for this is an accumulation of oxidation products.

Both S1 ('free' hydrocarbon) and S2 ('bound' hydrocarbon) decrease proportionately (by ~60%) in the leached zone (Fig. 8a). This suggests there is no preference to oxidation or that access to a component of S1, for example through an increase in porosity and permeability, is not improved during oxidation of pyrite. A component of S1 hydrocarbons may be completely sealed within organic pores and therefore inaccessible during pyrite oxidation. A small decrease to TOC between grade I and the grade II-B sample (~8% loss) indicates some OM has been completely removed from the outcrop, either oxidised or physically shed into suspension. The decrease to TOC contradicts the mapped relative increase in C abundance into Z1 alteration zones (Fig. 5f). However, the relative increase in C abundance is likely due to a decreased signal attenuation, since sulphides are absent in the Z1 zone.

The + 0.1‰ change in $\delta^{13}C_{org}$, regarding the coupled I with II-B samples (Fig. 8d), is close to the analytical error so interpretation is limited and most likely indicates no change in the isotopic composition of OM between fresh and altered samples. However, if the difference between grade I and II-B samples is reliable, this change indicates that the fresh fraction comprises slightly more isopically negative C; potentially OM of a marine origin (Lewan, 1986) that is typically more labile during weathering (e.g., Tyson, 1995). The pyrolized carbon fraction is more susceptible to oxidation than residual carbon, which remains constant regardless of weathering grade (Fig. 7e, f). Pyrolized carbon therefore represents the most labile fraction, but the process of accumulation of oxidation products could also convert some pyrolizable carbon into refractory carbon.

The organic characteristics of grade II-A samples from the stream section are indistinguishable from grade I samples. However, grade III-A samples from the slope are clearly distinguished from the fresh equivalent. The difference between the organic composition of grade II-A in the stream and slope requires explanation. Since meteoric waters potentially have differing capabilities to mobilise and concentrate elements (e.g., As; Section 5.1.2), it is plausible meteoric waters that percolate along fractures in the slope are more destructive to OM than in the stream section.

5.2. Physical processes

The absence of a leached zone immediately at the stream bed indicates that the rate of physical weathering is greater than the rate of chemical alteration. Physical weathering in the stream is likely driven by bedrock abrasion. Neither the Rock-Eval parameters or element concentrations exhibit any systematic changes with depth into the outcrop (away from fractures). This indicates that an outer leached zone above an oxidation 'front' which would be broadly parallel to the outcrop surface (e.g., Tuttle et al., 2009), is not present in either the stream or weathered slope. Therefore weathering at the study site is ultimately driven by physical, rather than chemical, weathering processes (Fig. 9). This emphasises the importance of chemical weathering processes operating in downstream reservoirs and within the soil profile, because the dominant export mechanism from the outcrop will be via downslope transport of particles. This is particularly relevant when weathering of OM is placed in the context of the global carbon cycle (e.g., Blair et al., 2003) and considering the fate of potentially toxic elements.

Physical weathering on the slope is likely driven by a combination of frost weathering, wetting-drying, thermal cycles and possibly even dilation effects due to deglaciation if considering the process over longer timescales (e.g. Hall, 2013). The lack of vegetation, lithobionts and only localised chemical alteration on the surfaces of grade IV 'paper shale', despite occurring immediately at the outcrop surface, suggests the slope is relatively fresh. Physical weathering on the slope promotes development of a relatively high fracture density when compared to the stream section, which are exploited by chemical alteration processes (see Section 5.1). A positive feedback mechanism is envisaged, because progressive chemical alteration along fracture surfaces may further enhance mechanical weathering by stress corrosion at fracture tips (Whalley et al., 1982). The volume increase associated with development of iron oxides along fractures in the slope may also promote fracturing.

Despite a lack of chemical alteration, grade IV samples are compositionally distinct compared to the majority of unweathered samples. Based on the compositional range from cores perpendicular to bedding (DC1A, DC1B, DC4), stratigraphic variation is a plausible explanation for the observed composition for grade IV samples. Alternatively, the observations could also relate to weathering. Determining whether this variation is simply stratigraphic, or relates to weathering (see Section 5.3), is challenging.

5.3. Slope bias

Since grade III-A, III-B, III-C and IV samples all exhibit systematic differences compared to the stream counterparts, this favours physical weathering as a driver for the compositional bias on the slope (Fig. 9). Evidence for this bias includes a higher Si/Al ratio suggesting greater biogenic silica content and/or lower clay content, higher TOC and higher Mo concentration for grade IV samples. The majority of other elements are depleted relative to grade I samples (Fig. 7). The slope bias process is described below. Physical and chemical weathering processes operate in a synergistic manner (Viles, 2013). These processes promote development of bedding-parallel fractures, which exploit planes of weakness in order to propagate into the slope. Planes of weakness are likely to be more porous and permeable layers. Widely spaced silty and clay-rich laminae are present throughout the studied section, and in some cases, incipient weathering fractures with secondary iron oxides are observed along these planes (Fig. 3b). Thus the development of the paper shale texture is biased because it exploits inherent weaknesses.

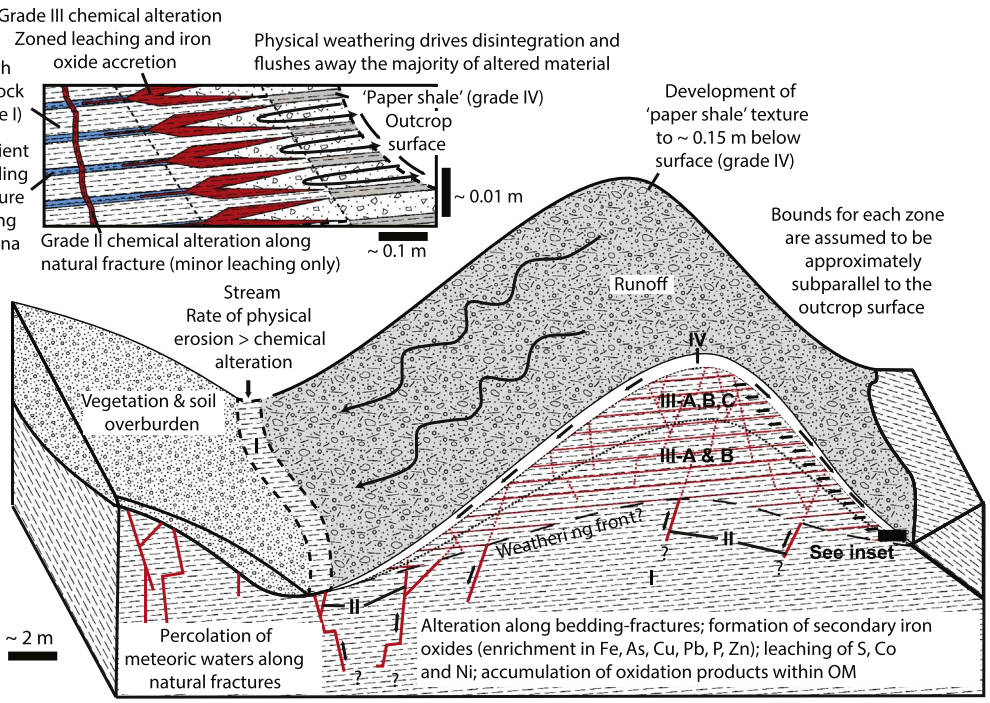

Fig. 9. Proposed model for weathering of outcrop in temperate climates for stream-cut and slope exposure. Fresh material (grade I) is exposed at the surface of streams. Chemical alteration as leached layers occurs along natural fracture surfaces (grade II), both in the stream and slope section. Chemical alteration as leached layers and precipitated goethite coatings is observed along bedding fractures on the slope (grade III). 'Paper shale' (grade IV) is chemically unaltered but is a potentially biased record due to propagation of fractures along laminae.

This process is comparable to the physical deterioration model for moderate strength rock with pre-existing 'flaws' defined by Nicholson and Nicholson (2000).

If weathering fractures consistently develop and propagate along laminae, the surfaces initially exposed to chemical alteration will be distinct compared the bulk sample composition. For example, some laminae comprise concentrations of relatively coarse (silt-sized) or clay-rich grains; these will be enriched in 'terrestrial' (detrital) elements and depleted in more 'marine' components compared to the bulk. As physical weathering processes progressively dominate the slope towards the outcrop surface, all alteration zones (Z1, Z2 and Z3) are disintegrated by physical weathering processes (Nicholson and Nicholson, 2000). Since fracture surfaces develop along laminae that are enriched in a more 'terrestrial' composition, this is the first unaltered fraction to be exposed. Once these surfaces disintegrate, particles are freed. These particles continue to be chemically altered and are ultimately transported downslope.

Continued disintegration produces clay to sand-sized particles comprising a mixture of altered and fresh material, which is ultimately washed downslope. 'Paper shale' (grade IV) represents the remaining chemically unaltered, yet biased, *in situ* mudstone record. Therefore mudstone sampled from the slope will not reflect the original bulk composition because some information has been lost during mechanical weathering. If not considered, this will result in a distorted picture of organic-rich mudstones. These errors could propagate into larger assessments, for example hydrocarbon source rock evaluations (Section 5.4), or palaeoenvironmental reconstructions, if based on field data.

Cs/Cu and OI are useful proxies for tracking the mudstone response to weathering, including the slope bias. Cs adsorbed onto detrital clay surfaces (e.g., Bostick et al., 2002) can be used as a proxy for presence of detrital laminae, and Cu fixed by OM in the water column (Tribovillard et al., 2006) can be used as a proxy for samples with fewer laminae. A strong positive correlation between Cs and Al ($r^2 = 0.84$), in addition to Ti, supports the assumption Cs is associated with the detrital clay fraction (Fig. 6a). Since grade II-A, grade II-B, III-A and III-B samples contain an excess of Cu relative to grade I samples, Cu is also a proxy for alteration prior to substantial development of iron oxide coatings and physical weathering. Fresh mudstone exhibits an initial composition with relatively low TOC (~3.5 wt%) and stable Cu/TOC (Fig. 10a). The relatively low TOC and Cu concentration reflects sampling of a mixture of organic (and Cu)-rich muds together with organic-poor detrital laminae. This mixture of sediment types is associated with a greater proportion of detrital elements, including Cs (Fig. 10b).

High Cs/Cu and low OI indicates truly unaltered composition, typical of material recovered from streams (Fig. 10c). Once mudstone is exposed to chemical weathering along fracture surfaces (both on the slope and in stream section), the composition trends towards low Cs/Cu and high OI. This indicates a chemically altered composition, primarily due to excess Cu within leached zones and an accumulation of oxidation products within the OM. Alteration in the vicinity of natural fractures within the stream section does not progress beyond this stage of chemical alteration.

The onset of physical weathering removes the overprint due to chemical weathering, and initially exploits laminae enriched in detrital components. Ultimately low Cs/Cu and low OI indicates samples have been subject to physical weathering and exhibit the slope bias. Whilst not observed, a high Cs/Cu and high OI would indicate a chemically altered sample with a significant detrital component. Since OI is also a proxy for the type of OM, relatively high Cs/Cu and OI could also indicate unaltered material but a dominance of Type III OM, which typically comprises terrestrially-derived OM such as phytoclasts and spores (e.g., Tyson, 1995). Relatively high Cs/Cu would also be expected in sediments abundant in Type III OM because Cs is detrital in origin.

Cs/Cu can therefore be used to complement other proxies for weathering of organic-rich mudstone deposited under anoxic or euxinic conditions (e.g., S/Fe, OI; Fig. 10d). This is particularly relevant for samples where interpretation of S/Fe is uncertain, for example, if a large proportion of unreactive Fe is present (Lyons and Severmann, 2006). In other environments of deposition (and palaeoredox conditions in bottom waters), the spacing, geometry and chemical composition of laminae will differ substantially from this study. Whilst a resulting bias on the slope is still expected, the magnitude and direction of change relative to the bulk geochemistry are uncertain and require further investigation.

5.4. Implications for analysis of outcrop samples

Perennial stream sections should be targeted rather than slope sections because unaltered material is exposed at the outcrop surface without bias. Completely unaltered material is difficult to extract from weathered slope sections, even when excavating by several tens of centimetres into the outcrop. This is primarily due to a high abundance of bedding fractures that are a conduit for oxidising meteroic waters, resulting in leaching and/or precipitation of iron oxide coatings. Iron oxide coatings are visually obvious, but leached layers are more subtle and may only be recognised using microscopy. Even if chemically unaltered material is recovered from the slope, sediment heterogeneity potentially introduces a paper shale bias (Section 5.3).

In the stream section, alteration is typically localised to < 2 millimetre-thick zones parallel to the natural fracture surfaces. Therefore this type of alteration can be avoided by sample screening or removed during preparation provided the natural fracture density is not too high (i.e., spacing < 5 mm). The orientation of natural fractures and bedding is an important factor when considering the suitability of a particular outcrop. Horizontal bedding greatly decreases the effective vertical permeability for meteoric water percolation. An outcrop cut by streams with horizontal bedding and a low natural fracture density are therefore preferable for sampling of fresh material.

Alteration along fractures is chemically distinctive, particularly for mudstones enriched in redox-sensitive elements and labile OM. Rock-Eval parameters exhibit a variety of sensitivities to weathering, with implications for hydrocarbon source rock assessments. TOC remains relatively resistant to chemical alteration, although this may be due to a low ratio of pyrolyzed C to residual C in these mudstones. The resistance of TOC to weathering is also dependent on mudstone composition (particularly sulphides; Section 1.1).

Despite relative stability of TOC, increases or decreases to other Rock-Eval parameters for chemically altered samples means interpretations could underestimate hydrocarbon potential, overestimate thermal maturity and skew assessment of organic composition towards the 'Type III' OM field (e.g., Tyson, 1995). However, the magnitude of change in Rock-Eval parameters between fresh and chemically altered samples is ultimately small (including OI), with the possible exception of T_{max}. Therefore Rock-Eval pyrolysis of chemically altered samples (of similar composition to the Bowland Shale) collected from similar outcrop settings are unlikely to make a significant difference from a hydrocarbon exploration perspective. Moreover, Rock-Eval pyrolysis data are never assessed in complete isolation from other datasets, and assuming chemically altered samples are atypical in a given dataset, these would be simply treated as anomalies and excluded from interpretation. However, if sample materials for source rock typing are thought to be chemically altered, a Rock-Eval back-calculation can be used to provide an indication of the original Rock-Eval parameters. This is especially robust if corroborated with an independent method for OM characterisation, such as palynology. T_{max} indicates an immature to early oil-window OM maturity. It is beyond the scope of this study to assess the susceptibility of OM to chemical alteration at higher thermal maturities.

The slope exposure described is comparable to many, but not all, other mudstone outcrops in the region. This is because many mudstone exposures are found adjacent to streams/rivers (e.g., Brandon et al., 1998), although some are related to slope failure, or are artificial (e.g., road cuttings). Common to all outcrop exposures is a relatively recent, or ongoing, period of physical removal of material. The age of the described outcrop probably post-dates the last glacial period, when glaciers covered the region (e.g., Brandon et al., 1998). The outcrop is therefore likely to be younger than ~13 ka. The apparent dominance of physical weathering processes is best explained by the two streams either side of the weathered slope (Fig. 2), rather than slope failure or an artificial origin. Since the last glaciation, the streams are likely to have maintained the relatively high slope gradient by incision, driving a relatively high rate of physical weathering across the slope. Therefore

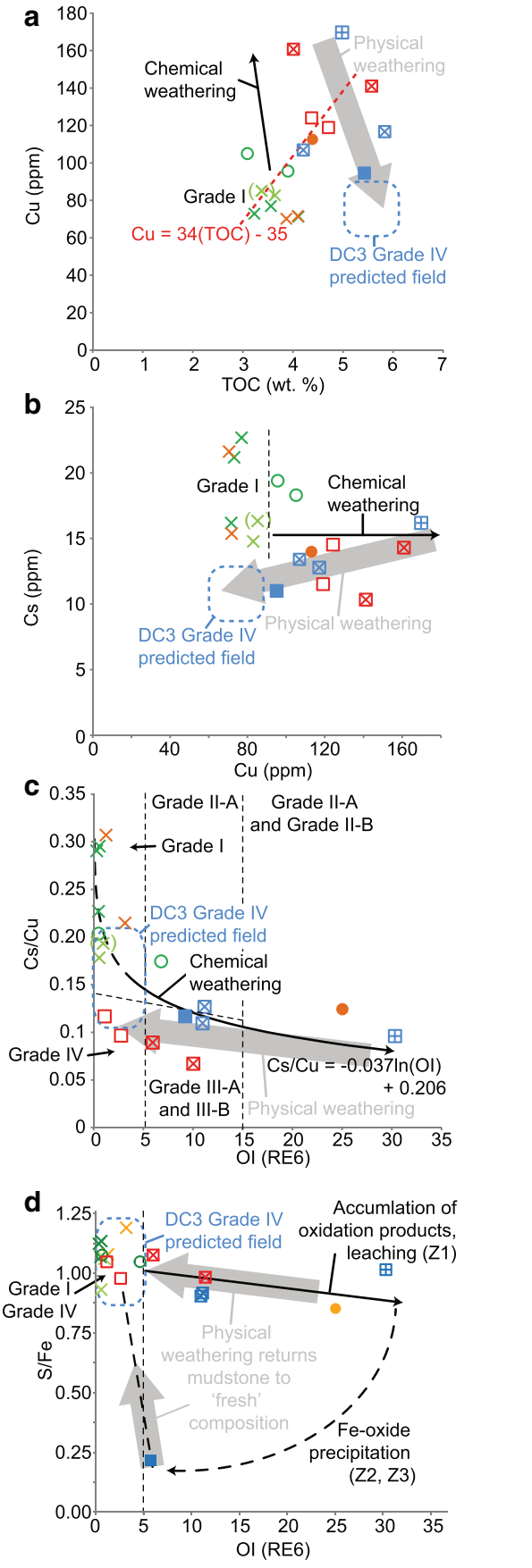

(caption on next page)

Fig. 10. (a) Cu versus TOC demonstrates covariance. (b) Cs versus Cu concentration plot differentiates grade I samples from all weathered samples along Cu ~ 90 ppm. Chemical weathering, by oxidation of pyrite and formation of iron oxides, increases the Cu concentration above the concentration related to organic matter content (see Fig. 4.0b). (c) Cs/Cu versus oxygen index (OI), used to differentiate weathering grades. (d) S/Fe versus OI also differentiates weathering grades. Legend as in Fig. 4.

the exposure of pristine grade IV material at the surface of the slope is likely due to a greater rate of physical weathering over surficial chemical alteration. Fischer et al. (2007) showed that leached layers on the surface of organic-rich rock exposed in temperate climates develop rapidly; typically over decades. On this basis, physical weathering on the slope is likely to be active, and dominant over chemical alteration, on this timescale.

Whilst physical weathering processes on the slope are probably active, some or all chemical alteration along fractures could represent relict features. This alteration potentially formed prior to outcrop exposure by deglaciation (including associated slope failure) or later stream incision. Whilst chemical alteration of organic-rich mudstones is generally thought to be limited during glaciations (e.g., Littke et al., 1991), the effect of direct glacial action will still induce chemical alteration (e.g., Anderson et al., 1997). For example, chemical alteration to several metres beneath outcrop surface was observed in an organic-rich mudstone outcrop in an Arctic climate (Georgiev et al., 2012), possibly related to the action of glacial groundwater. Following deglaciation or stream incision the outcrop became exposed at the surface, where physical weathering has dominated since.

The possibility that some chemical alteration features are relict is important for understanding the role of Quaternary glacial-interglacial cycles during weathering of organic-rich mudstones and link to modern carbon, sulphur and trace element cycling (e.g., Berner, 2006). If some, or all, chemical alteration along fractures are relict features, this also means the thickness and intensity of chemical alteration at a given outcrop is dependent on the spatial and temporal extent and type of glacial processes that operated during the last glacial period. Regardless of whether some or all of the observed chemical alteration are relict or presently forming, the sequence of alteration is expected to be the same in similarly eroding slope settings.

6. Conclusions

Four weathering grades (I-IV) are defined in a stream-cut and slope exposure of the organic-rich Bowland Shale in a temperate (western European) climate. Based on sedimentological, mineralogical, inorganic and organic geochemical analyses compared between stream and slope samples, we conclude that:

1. First-order perennial streams in temperate climates expose fresh (grade I) mudstone at the outcrop surface. This is likely because the rate of bedload abrasion is greater than the rate of chemical alteration;
2. Natural fractures may pose a challenge to sampling of unaltered material, because they are a conduit for oxidising meteoric waters that promote leaching of labile components (especially sulphides) adjacent to fractures (grade II). However, if fractures are widely spaced (i.e., > ~5 mm apart) and, as in this study, leached layers are typically < 2 mm thick, these can be avoided during sampling or removed during sample preparation;
3. Weathering on the slope generates additional bedding-parallel fractures that exploit heterogeneity in the original sedimentary fabric. Along bedding-parallel fractures, millimetre- to centimetre-scale leached layers and iron oxide coatings are widespread (grade III). Co and Ni are not hosted by secondary iron oxides and are therefore leached into meteoric waters (with S);
4. 'Paper shale' (grade IV) recovered from the weathered slope surface is not the most chemically altered, probably due to a dominance of physical over chemical weathering processes at the surface. Instead the most chemically altered mudstone on slopes is found several tens of centimetres into the outcrop, where the inferred rate of chemical alteration is greater than the rate of physical weathering. Although grade IV material sampled from the surface of the slope is primarily chemically unaltered, it potentially represents a biased record because the development of fractures is associated with initial sedimentary fabric heterogeneity (laminae). The direction and extent of this bias depends on the sedimentary fabric. The spacing, geometry and composition of laminae is particularly important, because the final composition of 'paper shale' will diverge or converge with the composition of laminae;
5. Chemically altered (grade II and III) outcrop samples exhibit lower concentrations of both 'free' (S1) and 'bound' (S2) hydrocarbon, lower TOC content, lower HI, elevated OI and elevated T_{max} relative to grade I samples. From an exploration perspective, the magnitude of change in Rock-Eval parameters between fresh and altered samples is relatively small. Therefore Rock-Eval pyrolysis of altered samples collected from similar lithologies, in similarly eroding slope settings, is unlikely to result in significant changes to the interpretation of OM composition and hydrocarbon generation potential. If analysis of chemically weathered samples is unavoidable, back-extrapolation of Rock-Eval parameters can assist in the estimation of pre-weathering organic compositions;
6. Together Cs/Cu and OI is a proxy for the progression of weathering through each grade.

Acknowledgements

This study was funded by the Natural Environment Research Council (NERC), [grant no. NE/L002493/1], within the Central England Training Alliance (CENTA) consortium. The study also received CASE funding from the British Geological Survey. Stable carbon isotope analyses were part-funded by the NERC Isotope Geosciences Facilities Steering Committee (NIGFSC) [IP-1566-1115]. Nick Riley (Carboniferous Ltd.) is thanked for sharing his expertise and assistance, particularly regarding the field identification of marine faunas. Charlotte Watts is thanked for providing field assistance. Nick Marsh, Tom Knott and Cheryl Haidon are thanked for providing expertise and assistance during inorganic geochemical and mineralogical analyses. Chris Kendrick helped with the production of the carbon isotope data.

Supplementary data

The R script used for statistical analyses and generation of plots is provided in Appendix I. The script can be used together with the Emmings et al. (2017) dataset. Method statements and major element concentration data, on an oxide wt% basis, are provided in Appendix II.

References

Amundson, R., 2005. Soil Formation, Surface and Ground Water, Weathering, and Soils. Elsevier Science, Amsterdam, GB. http://dx.doi.org/10.1016/B978-0-08-095975-7.00501-5.

Anderson, S., et al., 1997. Chemical weathering in glacial environments. Geology 25 (5), 399–402. http://dx.doi.org/10.1130/0091-7613(1997)025<0399:cwige>2.3.co;2.

Andrews, I.J., 2013. The Carboniferous Bowland Shale Gas Study: Geology and Resource Estimation. British Geological Survey for Department of Energy and Climate Change.

Arthurton, R.S., 1984. The Ribblesdale fold belt, NW England—a Dinantian-early Namurian dextral shear zone. Geol. Soc. Lond., Spec. Publ. 14 (1), 131–138. http://dx.doi.org/10.1144/gsl.sp.1984.014.01.13.

Berner, R.A., 2006. GEOCARBSULF: a combined model for Phanerozoic atmospheric O_2 and CO_2. Geochim. Cosmochim. Acta 70 (23), 5653–5664. http://dx.doi.org/10.1016/j.gca.2005.11.032.

Blair, N.E., et al., 2003. The persistence of memory: the fate of ancient sedimentary organic carbon in a modern sedimentary system. Geochim. Cosmochim. Acta 67 (1), 63–73. http://dx.doi.org/10.1016/S0016-7037(02)01043-8.

Bostick, B.C., et al., 2002. Cesium adsorption on clay minerals: an EXAFS spectroscopic investigation. Environ. Sci. Technol. 36 (12), 2670–2676. http://dx.doi.org/10.1021/es0156892.

Brandon, A., et al., 1998. Geology of the Country around Lancaster: Memoir for 1:50 000 Sheet 59. The Stationary Office, London.
Breward, N., et al., 2015. Anomalous enrichment of molybdenum and associated metals in Lower Jurassic (Lias Group) black shales of central England, as revealed by systematic geochemical surveys. Proc. Geol. Assoc. 126 (3), 346–366. http://dx.doi.org/10.1016/j.pgeola.2015.03.007.
Canty, A., 2002. Resampling Methods in R: The Boot Package. 2(3). R News, pp. 2–7.
Chung, N.C., Storey, J.D., 2015. Statistical significance of variables driving systematic variation in high-dimensional data. Bioinformatics 31 (4), 545–554. http://dx.doi.org/10.1093/bioinformatics/btu674.
Chung, N., et al., 2015. Jackstraw: Statistical Inference of Variables Driving Systematic Variation. R Package Version 1.1. http://CRAN.R-project.org/package=jackstraw.
Clayton, J., Swetland, P., 1977. Subaerial weathering of sedimentary organic matter. Geochim. Cosmochim. Acta 42, 305–312. http://dx.doi.org/10.1016/0016-7037(78)90183-7.
Davies, S.J., 2008. The record of Carboniferous sea-level change in low-latitude sedimentary successions from Britain and Ireland during the onset of the late Paleozoic ice age. Geol. Soc. Am. Spec. Pap. 441, 187–204. http://dx.doi.org/10.1130/2008.2441(13).
Davies, S.J., et al., 2012. Sedimentary process control on carbon isotope composition of sedimentary organic matter in an ancient shallow-water shelf succession. Geochem. Geophys. Geosyst. 13 (11), 1–15. http://dx.doi.org/10.1029/2012GC004218.
Dean, W.E., et al., 1986. Depletion of 13C in Cretaceous marine organic matter: Source, diagenetic, or environmental signal? Mar. Geol. 70 (1-2), 119–157. http://dx.doi.org/10.1016/0025-3227(86)90092-7.
Deroo, G., et al., 1980. Organic geochemistry of Cretaceous sediments at DSDP holes 417D (Leg 51), 418A (Leg 52), and 418B (Leg 53) in the Western North Atlantic. Initial Rep. Deep Sea Drill. Proj. 51 (52), 53. http://dx.doi.org/10.2973/dsdp.proc.515253.110.1980.
Dorn, R.I., 2013. 4.5 Rock Coatings A2 - Shroder, John F, Treatise on Geomorphology. Academic Press, San Diego, pp. 70–97. http://dx.doi.org/10.1016/B978-0-12-374739-6.00066-X.
Dyni, J., 2006. Geology and resources of some world oil-shale deposits. US Geol. Surv. Sci. Investig. Rep. 2005–5294, 42.
Emmings, J., et al., 2017. Data Accompanying: Stream and Slope Weathering Effects on Organic-rich Mudstone Geochemistry and Implications for Hydrocarbon Source Rock Assessment: A Bowland Shale Case Study. National Geoscience Data Centrehttp://dx.doi.org/10.5285/c39a32b2-1a30-4426-8389-2fae21ec60ad.
Fischer, C., Gaupp, R., 2005. Change of black shale organic material surface area during oxidative weathering: implications for rock-water surface evolution. Geochim. Cosmochim. Acta 69 (5), 1213–1224. http://dx.doi.org/10.1016/j.gca.2004.09.021.
Fischer, C., et al., 2007. Organic matter in black slate shows oxidative degradation within only a few decades. J. Sediment. Res. 77 (5), 355–365. http://dx.doi.org/10.2110/jsr.2007.041.
Fleming, G.A., Walsh, T., 1956. Selenium occurrence in certain Irish soils and its toxic effects on animals. Proc. R. Ir. Acad. B 58, 151–166.
Fraser, A., Gawthorpe, R., 2003. An atlas of Carboniferous Basin evolution in Northern England. In: Memoir 28. Geological Society, London. http://dx.doi.org/10.1144/GSL.MEM.2003.028.01.08.
Gawthorpe, R., 1987. Tectono-sedimentary evolution of the Bowland Basin, N England, during the Dinantian. J. Geol. Soc. 144, 59–71. http://dx.doi.org/10.1144/gsjgs.144.1.0059.
Georgiev, S., et al., 2012. Chemical signals for oxidative weathering predict Re–Os isochroneity in black shales, East Greenland. Chem. Geol. 324–325 (0), 108–121. http://dx.doi.org/10.1016/j.chemgeo.2012.01.003.
Goldich, S.S., 1938. A Study in Rock-Weathering. J. Geol. 46 (1), 17–58. http://dx.doi.org/10.2307/30079586.
Gross, D., et al., 2015. Organic geochemistry of Mississippian shales (Bowland Shale Formation) in central Britain: Implications for depositional environment, source rock and gas shale potential. Mar. Pet. Geol. 59 (0), 1–21. http://dx.doi.org/10.1016/j.marpetgeo.2014.07.022.
Guion, P.D., et al., 2000. Carboniferous sedimentation and volcanism on the Laurussian margin. In: Woodcock, N.H., Strachan, R. (Eds.), Geological History of Britain and Ireland. Wiley-Blackwell, Hoboken, USA, pp. 227–270. http://dx.doi.org/10.1002/9781118274064.ch14.
Hall, K., 2013. 4.15 Mechanical Weathering in Cold Regions A2 - Shroder, John F, Treatise on Geomorphology. Academic Press, San Diego, pp. 258–276. http://dx.doi.org/10.1016/B978-0-12-374739-6.00062-2.
Hallsworth, C.R., et al., 2000. Carboniferous sand provenance in the Pennine Basin, UK: constraints from heavy mineral and detrital zircon age data. Sediment. Geol. 137 (3), 147–185. http://dx.doi.org/10.1016/S0037-0738(00)00153-6.
Herbin, J., et al., 1983. Organic geochemistry in the Mesozoic and Cenozoic formations on Site 534, Leg 76, Blake-Bahama Basin, and comparison with Site 391, Leg 44. Initial Rep. Deep Sea Drill. Proj. 76. http://dx.doi.org/10.2973/dsdp.proc.76.117.1983.
Huerta-Diaz, M.A., Morse, J.W., 1992. Pyritization of trace metals in anoxic marine sediments. Geochim. Cosmochim. Acta 56 (7), 2681–2702. http://dx.doi.org/10.1016/0016-7037(92)90353-K0.
Johnson, C.C., et al., 2005. G-BASE: baseline geochemical mapping of Great Britain and Northern Ireland. Geochem. Explor. Environ. Anal. 5 (4), 347–357. http://dx.doi.org/10.1144/1467-7873/05-070.
Könitzer, S.F., et al., 2016. Significance of sedimentary organic matter input for shale gas generation potential of Mississippian Mudstones, Widmerpool Gulf, UK. Rev. Palaeobot. Palynol. 224 (Part 2), 146–168. http://dx.doi.org/10.1016/j.revpalbo.2015.10.003.
Lewan, M.D., 1986. Stable carbon isotopes of amorphous kerogens from Phanerozoic sedimentary rocks. Geochim. Cosmochim. Acta 50 (8), 1583–1591. http://dx.doi.org/10.1016/0016-7037(86)90121-3.
Leythaeuser, D., 1973. Effects of weathering on organic matter in shales. Geochim. Cosmochim. Acta 37, 113–120. http://dx.doi.org/10.1016/0016-7037(73)90249-4.
Littke, R., et al., 1991. Quantification of loss of calcite, pyrite, and organic matter due to weathering of Toarcian black shales and effects on kerogen and bitumen characteristics. Geochim. Cosmochim. Acta 55, 3369–3378. http://dx.doi.org/10.1016/0016-7037(91)90494-P.
Menning, M., et al., 2006. Global time scale and regional stratigraphic reference scales of Central and West Europe, East Europe, Tethys, South China, and North America as used in the Devonian–Carboniferous–Permian Correlation Chart 2003 (DCP 2003). Palaeogeogr. Palaeoclimatol. Palaeoecol. 240 (1–2), 318–372. http://dx.doi.org/10.1016/j.palaeo.2006.03.058.
Lyons, T.W., Severmann, S., 2006. A critical look at iron paleoredox proxies: New insights from modern euxinic marine basins. Geochim. Cosmochim. Acta 70 (23), 5698–5722. http://dx.doi.org/10.1016/j.gca.2006.08.021.
Mitchell, K., et al., 2012. Selenium as paleo-oceanographic proxy: a first assessment. Geochim. Cosmochim. Acta 89, 302–317. http://dx.doi.org/10.1016/j.gca.2012.03.038.
Nicholson, D.T., Nicholson, F.H., 2000. Physical deterioration of sedimentary rocks subjected to experimental freeze–thaw weathering. Earth Surf. Process. Landf. 25 (12), 1295–1307. http://dx.doi.org/10.1002/1096-9837(200011)25:12<1295::AID-ESP138>3.0.CO;2-E.
Norry, M.J., et al., 1994. Mineralogy and geochemistry of the Peterborough Member, Oxford Clay Formation, Jurassic, UK: element fractionation during mudrock sedimentation. J. Geol. Soc. 151 (1), 195–207. http://dx.doi.org/10.1144/gsjgs.151.1.0195.
Oguchi, C.T., 2013. 4.6 Weathering Rinds: Formation Processes and Weathering Rates A2 - Shroder, John F, Treatise on Geomorphology. Academic Press, San Diego, pp. 98–110. http://dx.doi.org/10.1016/B978-0-12-374739-6.00067-1.
Oksanen, J., et al., 2016. Vegan: Community Ecology Package. R Package Version 2.3-3. http://CRAN.R-project.org/package=vegan.
Parnell, J., et al., 2016. Selenium enrichment in Carboniferous Shales, Britain and Ireland: problem or opportunity for shale gas extraction? Appl. Geochem. 66, 82–87. http://dx.doi.org/10.1016/j.apgeochem.2015.12.008.
Peak, D., et al., 2006. Selenite adsorption mechanisms on pure and coated montmorillonite: an EXAFS and XANES spectroscopic study. Soil Sci. Soc. Am. J. 70 (1), 192–203. http://dx.doi.org/10.2136/sssaj2005.0054.
Petsch, S.T., 2014. 12.8 - weathering of organic carbon A2 - Holland, Heinrich D. In: Turekian, K.K. (Ed.), Treatise on Geochemistry, second edition. Elsevier, Oxford, pp. 217–238. http://dx.doi.org/10.1016/B978-0-08-095975-7.01013-5.
Petsch, S.T., et al., 2000. A field study of the chemical weathering of ancient sedimentary organic matter. Org. Geochem. 31 (5), 475–487. http://dx.doi.org/10.1016/S0146-6380(00)00014-0.
Plant, J., Jones, D., 1989. Metallogenic models and exploration criteria for buried carbonate-hosted ore deposits - a multidisciplinary study in eastern England. Keyworth, Nottingham: British Geological Survey; London: The Institution of Mining and Metallurgy. Springer Science and Business Media Dordrecht. 10.1007%2F978-3-642-51858-4_18.
Poppe, L., et al., 2001. A Laboratory Manual for X-Ray Powder Diffraction. U.S. Geological Survey Open-file Report, 01-041.
R, Core Team, 2015. R: A Language and Environment for Statistical Computing. R Foundation for Statistical Computing. https://www.R-project.org.
Raiswell, R., et al., 1988. Degree of pyritization of iron as a paleoenvironmental indicator of bottom-water oxygenation. J. Sediment. Res. 58 (5), 812–819. http://dx.doi.org/10.1306/212f8e72-2b24-11d7-8648000102c1865d.
Ramsbottom, W.H.C., 1977. Major cycles of transgression and regression (mesothems) in the Namurian. Proc. Yorks. Geol. Soc. 41 (3), 261–291. http://dx.doi.org/10.1144/pygs.41.3.261.
Ramsbottom, W.H.C., Saunders, W.B., 1985. Evolution and evolutionary biostratigraphy of Carboniferous ammonoids. J. Paleontol. 59 (1), 123–139. http://dx.doi.org/10.2307/1304831.
Robertson, F.N., 1989. Arsenic in ground-water under oxidizing conditions, south-west United States. Environ. Geochem. Health 11 (3-4), 171–185. http://dx.doi.org/10.1007/bf01758668.
Small, E.E., et al., 2015. Variability of rock erodibility in bedrock-floored stream channels based on abrasion mill experiments. J. Geophys. Res. Earth Surf. 120 (8), 1455–1469. http://dx.doi.org/10.1002/2015JF003506.
Starmer, J., 2015. pcaBootPlot: Create 2D Principal Component Plots With Bootstrapping. R Package Version 0.2.0. http://CRAN.R-project.org/package=pcaBootPlot.
Stuart, M., 2012. Potential groundwater impact from exploitation of shale gas in the UK. In: Groundwater Science Programme, Open Report OR/12/001, . http://nora.nerc.ac.uk/16467/.
Taylor, S., McLennan, S., 1985. The Continental Crust: Its Composition and Evolution. Blackwell Scientific, London (312 pp.).
Tribovillard, N., et al., 2006. Trace metals as paleoredox and paleoproductivity proxies: an update. Chem. Geol. 232, 12–32. http://dx.doi.org/10.1016/j.chemgeo.2006.02.012.
Tuttle, M., et al., 2009. Weathering of the New Albany Shale, Kentucky: II. Redistribution of minor and trace elements. Appl. Geochem. 24 (8), 1565–1578. http://dx.doi.org/10.1016/j.apgeochem.2009.04.034.
Tyson, R., 1995. Sedimentary Organic Matter: Organic Facies and Palynofacies. London. https://doi.org/10.1007%2F978-94-011-0739-6.
Velde, B., Meunier, A., 1987. Petrologic Phase Equilibria in Natural Clay Systems, Chemistry of Clays and Clay Minerals, Mineralogical Society Monograph 6. Longman Scientific and Technical and the Mineralogical Society, pp. 423–458.

Viles, H.A., 2013. 4.2 Synergistic Weathering Processes A2 - Shroder, John F, Treatise on Geomorphology. Academic Press, San Diego, pp. 12–26. http://dx.doi.org/10.1016/B978-0-12-374739-6.00057-9.

Waters, C.N., Condon, D.J., 2012. Nature and timing of Late Mississippian to Mid-Pennsylvanian glacio-eustatic sea-level changes of the Pennine Basin, UK. J. Geol. Soc. 169 (1), 37–51. http://dx.doi.org/10.1144/0016-76492011-047.

Waters, C.N., Davies, S.J., 2006. Carboniferous: extensional basins, advancing deltas and coal swamps. In: Brenchley, P.J. (Ed.), The geology of England and Wales. Geological Society of London, London, England, pp. 173–223.

Waters, C.N., et al., 2007. Lithostratigraphical framework for Carboniferous successions of Great Britain (Onshore). In: British Geological Survey Research Report, RR/07/01.

Wedepohl, H., 1995. The composition of the continental crust. Geochim. Cosmochim. Acta 59 (7), 1217–1232. http://dx.doi.org/10.1016/0016-7037(95)00038-2.

Whalley, W., et al., 1982. Crack propagation and associated weathering in igneous rocks. Z. Geomorphol. 26 (1), 33–54.

White, A., Buss, H., 2013. Natural Weathering Rates of Silicate Minerals. In: Drever, J.I. (Ed.), Treatise on Geochemistry: Surface and Groundwater, Weathering and Soils. Elsevier Science Ltd., pp. 115–155. http://dx.doi.org/10.1016/B978-0-08-095975-7.00504-0.

Wildman, R., et al., 2004. The weathering of sedimentary organic matter as a control on atmospheric O_2: I. Analysis of a Black Shale. Am. J. Sci. 304, 234–249. http://dx.doi.org/10.2475/ajs.304.3.234.